Ivan Antolović, Jadran Vrabec

Vapor–liquid–liquid equilibria of nitrogen + ethane by molecular simulation

Citation details
Antolović, I., Vrabec, J. (2022). Vapor–Liquid–Liquid Equilibria of Nitrogen + Ethane by Molecular Simulation. In Industrial amp; Engineering Chemistry Research (Vol. 61, Issue 8, pp. 3104–3112). American Chemical Society (ACS). https://doi.org/10.1021/acs.iecr.1c04726.

Vapor-Liquid-Liquid Equilibria of Nitrogen + Ethane by Molecular Simulation

Ivan Antolović and Jadran Vrabec*

Thermodynamics and Process Engineering, Technical University Berlin, 10587 Berlin, Germany

E-mail: vrabec@tu-berlin.de

Phone: +49 30 314 22755

Abstract

Vapor-liquid, liquid-liquid and vapor-liquid-liquid equilibria of the binary system nitrogen + ethane are investigated systematically for temperatures between 105 and 260 K and pressures between 15 and 150 bar. Force fields models are used that have been parameterized beforehand solely to vapor-liquid equilibrium data and are augmented by a single binary parameter $\xi = 0.974$ that has also been adjusted in a preceding work to vapor-liquid equilibrium data at 260 K. The molecular mixture model is tested with a focus on its predictive power with respect to liquid-liquid equilibria. For that purpose, more than 4000 state points are sampled around the three-phase curve with molecular simulations in the isobaric-isothermal (NpT) and canonic (NVT) ensemble. Despite the large distance from its original adjustment point, the mixture model yields sound results for vapor-liquid equilibria at low temperatures and is capable of predicting the large miscibility gap of nitrogen + ethane with an average deviation of $\pm 0.025\,\mathrm{mol\,mol^{-1}}$. Furthermore, the thermodynamic factor is sampled with Kirkwood-Buff integration and is also used for phase equilibrium calculations. The simulation results are compared

with the high-accuracy multifluid GERG-2008 equation of state (EOS) and the Peng-Robinson EOS.

Introduction

Liquid mixtures of simple molecules continue to be of major importance in thermodynamics, not only because of their direct use in industrial processes, but also because they are particularly suitable for theoretical studies of the liquid phase. They provide an excellent testing ground for statistical theories and are thus helpful in gaining more insight into the molecular scale that governs the macroscopic behavior. Simple molecules are often described by spherically symmetrical intermolecular potentials where pairwise additivity is assumed. Ethane is an example of a linear molecule with a small elongation, whereas nitrogen is an even smaller and more compact molecule. Thus, the binary mixture nitrogen + ethane is a system comprised of simple molecules that is particularly interesting because it has a rather complex fluid phase behavior, exhibiting liquid-liquid equilibria (LLE) with a large miscibility gap at low temperatures.

Romig and Hanley[1] have shown that nitrogen + ethane is a Type III system according to the classification scheme introduced by van Konynenburg and Scott[2] (cf. Fig. 1a) or a 1^C1^Z system according to the more refined scheme of Bolz et al.[3]. The essential characteristic of Type III or 1^C1^Z systems is that the critical points of the two components are not connected with a continuous critical line. Instead, the critical line is interrupted by a three-phase locus, which lies between the two vapor pressure curves (cf. Fig. 1a). The phase boundaries in the pressure-mole fraction (p-x) and temperature-mole fraction (T-x) diagrams thus undergo remarkable shape transformations upon temperature and pressure variations (cf. Fig. 1b and 1c).

There are several experimental studies that have investigated vapor-liquid equilibria (VLE) of nitrogen + ethane.[4–9] Even though the VLE of this system is rather well-studied

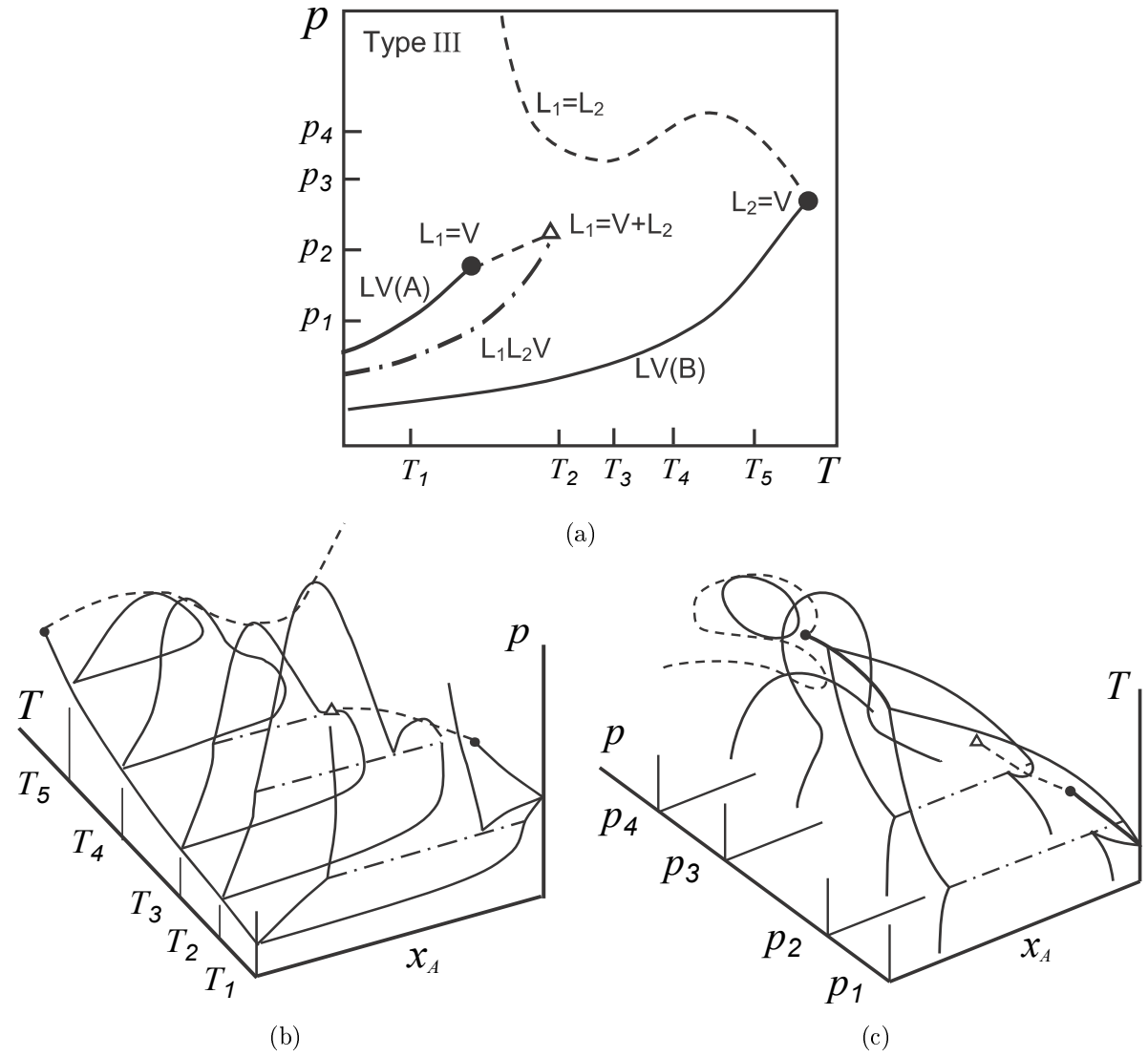

Figure 1: Schematic diagrams for Type III phase behavior: (a) Scott–van Konynenburg p–T projection, (b) p–x–y (T) space and (c) T–x–y (p) space.

for some time, experiments have still been carried out more recently to close gaps in certain temperature, pressure or composition ranges.[10,11] Considerably less has been published on liquid-liquid equilibria (LLE) of this mixture. The most comprehensive investigation was made by Wisotzki and Schneider[12], who measured lines of constant composition (isopleths) at temperatures as low as 88 K and pressures of up to 200 MPa. However, substantially more data are available at low temperature and moderate pressure, where the system is known to exhibit three-phase vapor-liquid-liquid equilibria (VLLE).[13–15] VLLE are thus a good starting point for obtaining and comparing LLE results.

Beside experimental and theoretical[1,16] investigations, molecular modeling and simulation offers an alternative approach for predicting phase equilibria. Previous works from our group[17,18] and others[19,20] have demonstrated its good predictive power regarding VLE of both pure fluids and their mixtures. Other authors have shown that this approach can also be utilized for LLE,[21–24] but only relatively few studies have been conducted for this type of phase equilibrium despite its importance for chemical separation processes, in particular extraction. Stoll et al.[18] successfully simulated the VLE of nitrogen + ethane by using pure component models[17] and adjusting a single state-independent binary parameter, namely $\xi = 0.974$ of the modified Berthelot combining rule. This parameter adjustment was carried out on the basis of a single experimental VLE state point at $T = 260$ K, making the approach both simple and concise, while still having a good predictive power.

Although VLE of nitrogen + ethane have been the subject of numerous simulation studies,[17–20] there have been no investigations of its LLE or VLLE with this approach. The objective of this work is to fill this gap and to extend the previous VLE research to the VLLE region and also to test whether the adjustment of a single parameter ξ to the VLE is sufficient to yield sound results for the miscibility gap under conditions far away from the original adjustment point. The simulation results are compared to GERG-2008,[25] a large empirical multi-parameter equation of state (EOS), and the Peng-Robinson EOS.[26]

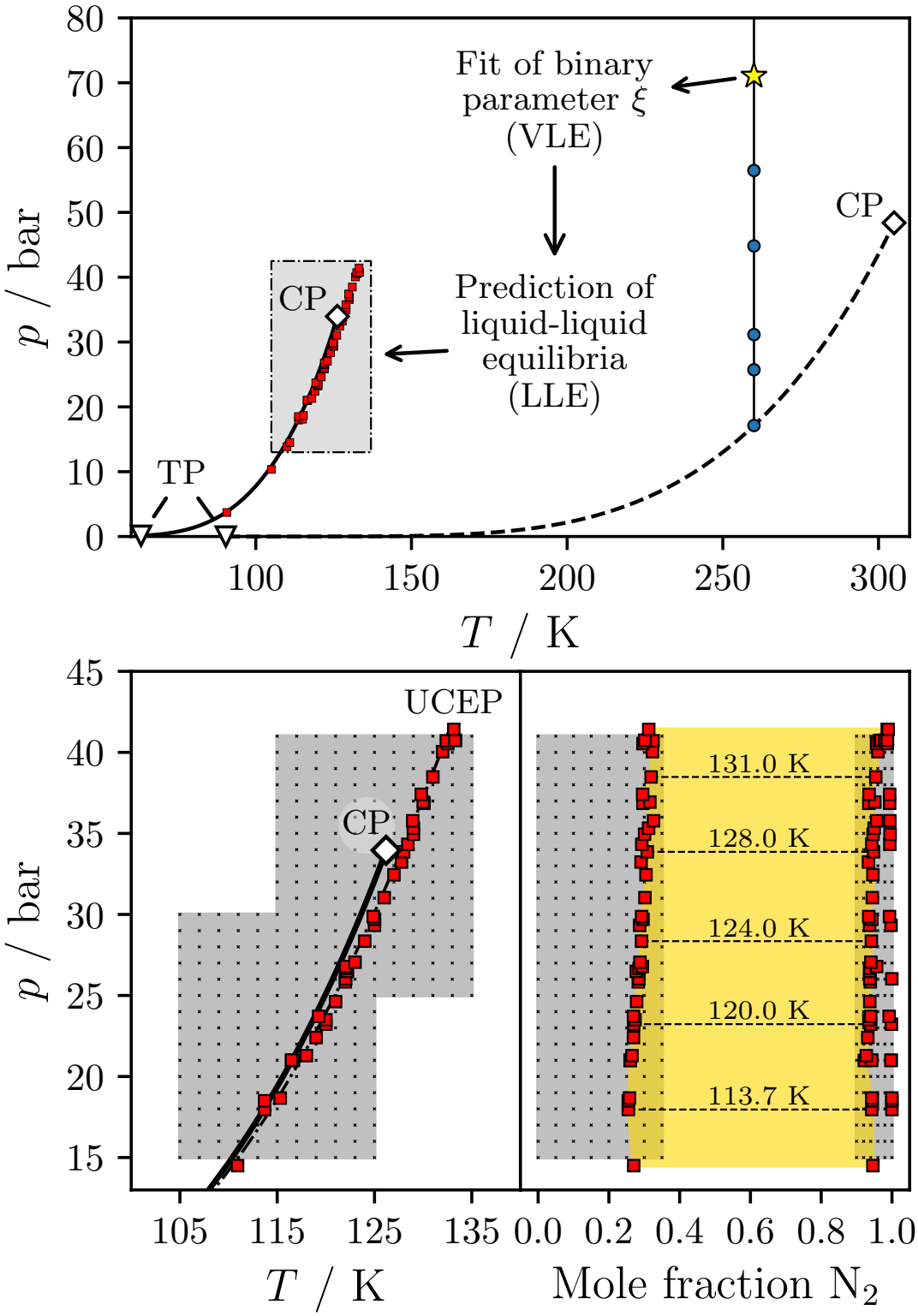

Figure 2: Principle of this work moving from VLE to LLE in the pressure-temperature diagram for nitrogen + ethane (top); a fine-meshed matrix of state points (black crosses in the gray area) was simulated around the three-phase curve (dashdotted line) in the p-T and p-x diagrams (bottom). Vapor pressure: nitrogen (solid line), ethane (dashed line). Yellow area: miscibility gap. Experimental data: VLE[27] (blue circles); VLLE[28–35] (red squares).

Molecular Simulation

Matrix of State Points

The working principle of this work is shown in Fig. 2 (top). Starting from the state point of binary parameter adjustment, phase equilibria were simulated for decreasing temperature until the three-phase curve was reached. As the natural transition line between VLE and LLE, the three-phase curve lends itself to predicting LLE with molecular models that have only been adjusted to VLE. Therefore, the main focus of this work was laid on the region around the three-phase curve including its upper critical endpoint (UCEP). A fine-meshed matrix of state points was set up around the VLLE between $p = 15$ and 41 bar with increments of $\Delta p = 1$ bar and between $T = 105$ and 135 K with increments of $\Delta T = 2$ K, resulting in a total of 4000 distinct simulation runs in this region (see Fig. 2 bottom). Since the experimental data indicate that the miscibility gap is at $x^{\mathrm{I}}_{\mathrm{N2}} \leq 0.32\,\mathrm{mol\,mol^{-1}}$ in the ethane-rich phase (I) and $x^{\mathrm{II}}_{\mathrm{N2}} \geq 0.92\,\mathrm{mol\,mol^{-1}}$ in the nitrogen-rich phase (II), the mole fraction was discretized between $x^{\mathrm{I}}_{\mathrm{N2}} = 0...0.35\,\mathrm{mol\,mol^{-1}}$ and $x^{\mathrm{II}}_{\mathrm{N2}} = 0.9...1\,\mathrm{mol\,mol^{-1}}$ with a step size of $\Delta x^{\mathrm{I}} = 0.05\,\mathrm{mol\,mol^{-1}}$ and $\Delta x^{\mathrm{II}} = 0.02\,\mathrm{mol\,mol^{-1}}$, respectively. This ensured that both phases I and II were covered thoroughly, while avoiding physically meaningless solutions in the unstable region.

Simulation Details

All molecular simulation runs were carried out with the program $ms2$.[36–39] A cubic volume was assumed with periodic boundary conditions containing up to 4000 molecules. The intermolecular interactions were explicitly evaluated within a cutoff radius of 14 Å, considering analytical LJ long-range corrections with the angle-averaging method of Lustig[40]. The LLE simulations were conducted in two consecutive steps: (1) Monte Carlo (MC) simulations in the isobaric-isothermal (NpT) ensemble to obtain the density and (2) Molecular Dynamics (MD) simulations in the canonic (NVT) ensemble to obtain the chemical potentials

and the thermodynamic factor through Kirkwood-Buff integrals (KBI).[41] Simulations in the NVT ensemble were first equilibrated over $3 \cdot 10^5$ time steps, followed by production runs of $1.5 \cdot 10^7$ time steps. Newton's equations of motion were solved with a fifth-order Gear predictor-corrector numerical integrator and an integration time step of 1 fs. The chemical potentials were the primary property for determining phase equilibria and were sampled with Widom's test particle insertion method[42] using 4000 test particles per time step. The thermodynamic factor was calculated with KBI based on RDF that was sampled beyond the cutoff radius up to $L/2$ of the edge length of the cubic simulation volume with a sampling frequency of one per time step. Further simulation details are given in the supporting information.

Molecular Models

The employed molecular force field models for nitrogen and ethane were developed in a preceding work[17] on the basis of experimental VLE data of the pure fluids. Both components were modeled with the symmetrical two-center Lennard-Jones plus pointquadrupole pair potential (2CLJQ), which is a powerful model for small quadrupolar molecules. These models are rigid, non-polarizable and of united-atom type. The 2CLJQ model parameters for the pure fluids considered in this work are listed in Table 1. Interactions between unlike LJ sites were described by the modified Lorentz-Berthelot combining rules[43,44]

$$\sigma_{AB} = \frac{\sigma_A + \sigma_B}{2}, \tag{1}$$

$$\epsilon_{AB} = \xi \cdot \sqrt{\epsilon_A \cdot \epsilon_B}, \tag{2}$$

where $\xi = 0.974$ is a binary parameter that was adjusted in Ref. 18.

Table 1: Potential model (2CLJQ) parameters for nitrogen and ethane.[17]

Fluid	σ/Å	(ϵ/k_B)/K	L/Å	Q/DÅ
N_2	3.3211	34.897	1.0464	1.4397
C_2H_6	3.4896	136.99	2.3762	0.8277

Calculating Phase Equilibria

For an equilibrium, it is necessary that the coexisting phases (denoted as I and II) have the same temperature, the same pressure and also the chemical potentials of all components have to be equal:

$$T^{\mathrm{I}} = T^{\mathrm{II}}, \tag{3}$$

$$p^{\mathrm{I}} = p^{\mathrm{II}}, \tag{4}$$

$$\mu_i^{\mathrm{I}} = \mu_i^{\mathrm{II}}, \qquad \forall \quad i = 1, 2. \tag{5}$$

Many solution strategies have been proposed during the last century and still continue to be developed.[45–50] Depending on the variables that are being specified, a solution strategy might be assigned to one of the following two equivalent concepts: the μ-p or the μ-x concept.

μ-p Concept

For a given temperature T and mole fraction of one phase x_i^{I}, the chemicals potential μ_i^{I} are solely a function of pressure. Finding the phase equilibrium by meeting conditions (4) and (5) is then reduced to finding the mole fraction x_i^{II} of the other phase for which the chemical potentials of both phases intersect at one pressure, namely the vapor pressure p_σ. This thermodynamic concept is utilized for example by the NpT + test particle method[51,52] and in a more general fashion by the grand equilibrium (GE) method[53] which was applied in this work. The GE method starts by sampling the liquid phase with the goal to obtain an expression for the chemical potentials $\mu_i^L(p)$ as a function of pressure. At a given T,

x_i, p^L only one NpT simulation run is needed to achieve this goal, since the $\mu_i^L(p)$ can be approximated by a first-order Taylor series expansion

$$\mu_i^L(p) \approx \mu_i^L(p^L) + v_i^L(p^L)(p - p^L)/(k_B T), \tag{6}$$

where $v_i^L(p^L)$ is the partial molar volume of component i in the liquid phase and p^L is the pressure where the liquid was sampled. Subsequently, the vapor phase is simulated in a pseudo grand canonical ensemble (pseudo-μVT), directly leading to the saturated vapor state.

μ-x Concept

A different, but equivalent approach is given by the μ-x concept. For a specified temperature and pressure, the objective is to find the mole fractions x_i^{I} and x_i^{II} where the phase equilibrium condition (5) is satisfied. The chemical potential of component i can be expressed as

$$\mu_i = \mu_{0i} + RT \ln (x_i \gamma_i) , \tag{7}$$

where μ_{0i} is the chemical potential of the pure component at the same temperature and pressure, while γ_i is the activity coefficient. The chemical potential in Eq. (7) cannot be approximated by a linear function as before in the μ-p concept, but a suitable excess Gibbs energy model has to be adjusted. In this work, the NRTL model[54] was primarily used for this purpose. The second summand in Eq. (7) describes the deviation from the pure component chemical potential μ_{0i} and can be used to calculate the Gibbs energy of mixing

$$\frac{g^{\mathrm{mix}}}{RT} = \sum_i x_i \ln (x_i \gamma_i) . \tag{8}$$

Equation (5) then becomes

$$\left(\frac{\partial g^{\mathrm{mix}}}{\partial x_i} \right)_{T,p}^{\mathrm{I}} = \left(\frac{\partial g^{\mathrm{mix}}}{\partial x_i} \right)_{T,p}^{\mathrm{II}} . \tag{9}$$

Under phase equilibrium conditions, not only the chemical potentials have the same value, but also the slope of g^{mix} as a function of mole fraction must be equal in both phases. Therefore, finding the phase equilibrium is equivalent to identifying a tangent line that touches g^{mix} at two distinct contact points, namely at x_i^{I} and x_i^{II}.

An example as well as a comparison of both concepts is provided in the supporting information. The μ-x concept was found to be more reliable and robust for the purpose of this work to calculate LLE than the μ-p concept. This was mainly due to glancing intersections that occur at high density state points such as liquid-liquid phase equilibria. The occurrence of glancing intersections is described more thoroughly in the supporting information.

Three-Phase Equilibria

For a three-phase equilibrium, Eqs. (3) to (5) and (9) still hold, only an additional phase has to be considered. At constant temperature and pressure, the equilibrium condition for the coexisting phases (denoted as L1, L2, and V) reads

$$\mu_i^{\mathrm{L1}} = \mu_i^{\mathrm{L2}} = \mu_i^{\mathrm{V}}, \qquad \forall \quad i = 1, 2 \tag{10}$$

or

$$\left(\frac{\partial g^{\mathrm{mix}}}{\partial x_i}\right)_{T,p}^{\mathrm{L1}} = \left(\frac{\partial g^{\mathrm{mix}}}{\partial x_i}\right)_{T,p}^{\mathrm{L2}} = \left(\frac{\partial g^{\mathrm{mix}}}{\partial x_i}\right)_{T,p}^{\mathrm{V}}, \tag{11}$$

respectively. Therefore, the calculation of the three-phase equilibrium can analogously be performed with both the μ-p and μ-x concepts. Examples are provided in the supporting information.

Spinodal Curve and Thermodynamic Factor

The stability of phases ceases to exist between the spinodals, where

$$\left(\frac{\partial \mu_i}{\partial x_i}\right)_{T,p} = \left(\frac{\partial^2 g^{\mathrm{mix}}}{\partial x_i^2}\right)_{T,p} = 0. \tag{12}$$

Therefore, identifying a spinodal is equivalent to finding a composition where the thermodynamic factor vanishes

$$\Gamma = \frac{x_i}{RT}\left(\frac{\partial \mu_i}{\partial x_i}\right)_{T,p} = 0. \tag{13}$$

Equation (13) shows the relation between the chemical potential μ_i and the thermodynamic factor Γ. Thus, both variables can be used for adjusting a suitable g^{E} model. As Eq. (13) allows to convert μ_i and Γ into one another, it follows that the phase equilibrium cannot only be calculated from μ_i but also from Γ. Recently, the thermodynamic factor has been made accessible in the simulation tool $ms2$ by incorporating Kirkwood-Buff integration (KBI).[55] Since both the chemical potentials and the thermodynamic factor were obtained independently by different methods, they lend themselves for comparison, as discussed below.

Results

Vapor-Liquid Equilibria

Figure 3 (left) shows a comparison between the simulation results and the experimental data at $T = 200$, 230 and 260 K, together with the GERG-2008 and Peng-Robinson EOS.

The simulation results are in very good agreement with the experimental data and the EOS over a major part of the phase envelope, especially at $T = 260$ K where the binary parameter ξ has been adjusted. However, even at such relatively high temperatures, it can be noticed that the simulation data start to deviate from the experimental values the closer they are to the critical point and the lower the temperature is. This can be seen more clearly

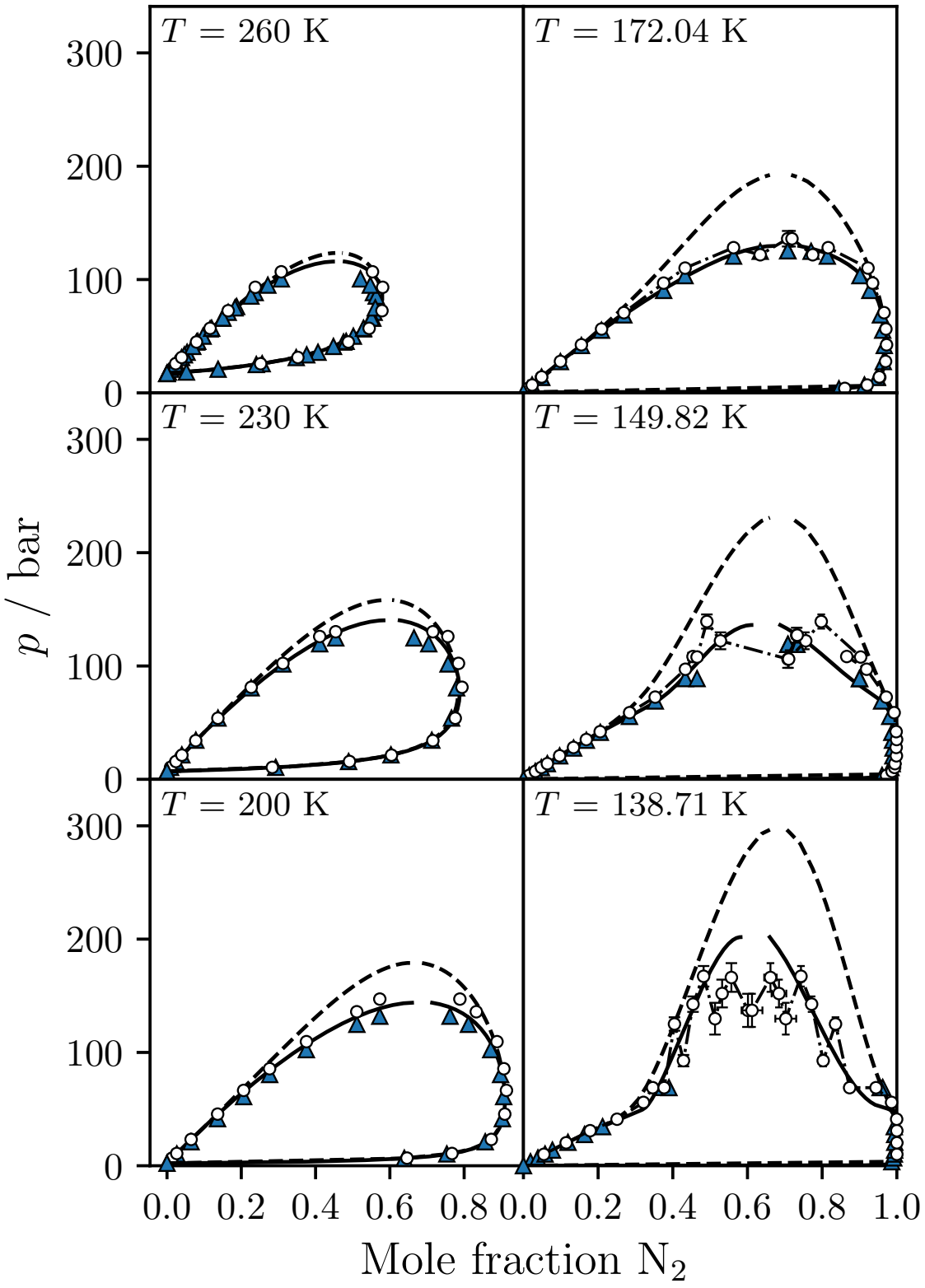

Figure 3: Pressure-mole fraction phase diagram of nitrogen + ethane at (left): T = 260, 230 and 200 K and (right): T = 172.04, 149.82 and 138.71 K. Circles: simulation data; blue triangles: experimental VLE data;[27,56–58] solid line: GERG-2008 EOS;[25] dashed line: Peng-Robinson EOS.

in Fig. 3 (right) for decreasing temperature $T = 172.04$, 149.82 and 138.71 K. By further reducing the temperature and moving in the direction of the three-phase region, the phase envelope begins to transform its shape. LLE emerge and separate from the VLE envelope, narrowing down at the top of the envelope such that the critical point moves to a higher pressure. Again, it can be seen that even though the simulation results agree very well for lower pressures, they increasingly deviate where the LLE forms.

Liquid-Liquid Equilibria

All simulations at or below the UCEP were evaluated with the μ-x concept which is capable to yield results both at constant temperature (p-x diagrams) and at constant pressure (T-x diagrams). Figure 4 shows a compilation of LLE results in the p-x (top) and the T-x (bottom) plane. Both the binodal and spinodal are shown to highlight the metastable and unstable regions. It can be seen that the expected large miscibility gap was predicted well by simulation, although it is somewhat larger than the experimental data suggest. However, the data points are very close to the binodal or at least somewhere between the binodal and spinodal curves, but always within the predicted metastable region. This is a good indication that the simulations yield reasonable results and are able to predict physically sound and stable liquid-liquid equilibria for this system.

The ethane-rich phase (I) is in some cases even quantitatively well predicted with an average deviation in the mole fraction of less than $0.02\,\mathrm{mol\,mol^{-1}}$, whereas the solutions for the nitrogen-rich phase (II) tend towards slightly higher mole fractions compared to the experimental data. Deviations that arise in both phases might be assigned to the molecular model, which relies only on a single state-independent binary parameter ξ or they can equally be the consequence of an inadequacy of the NRTL model. A comprehensive overview of all p-x and T-x diagrams is given in the supporting information.

To quantify the difference between simulation and experiment with respect to LLE, the absolute deviation $x_{\mathrm{N2}}^{\mathrm{sim}} - x_{\mathrm{N2}}^{\mathrm{exp}}$ for phases I and II is shown in Fig. 5. For a better repre-

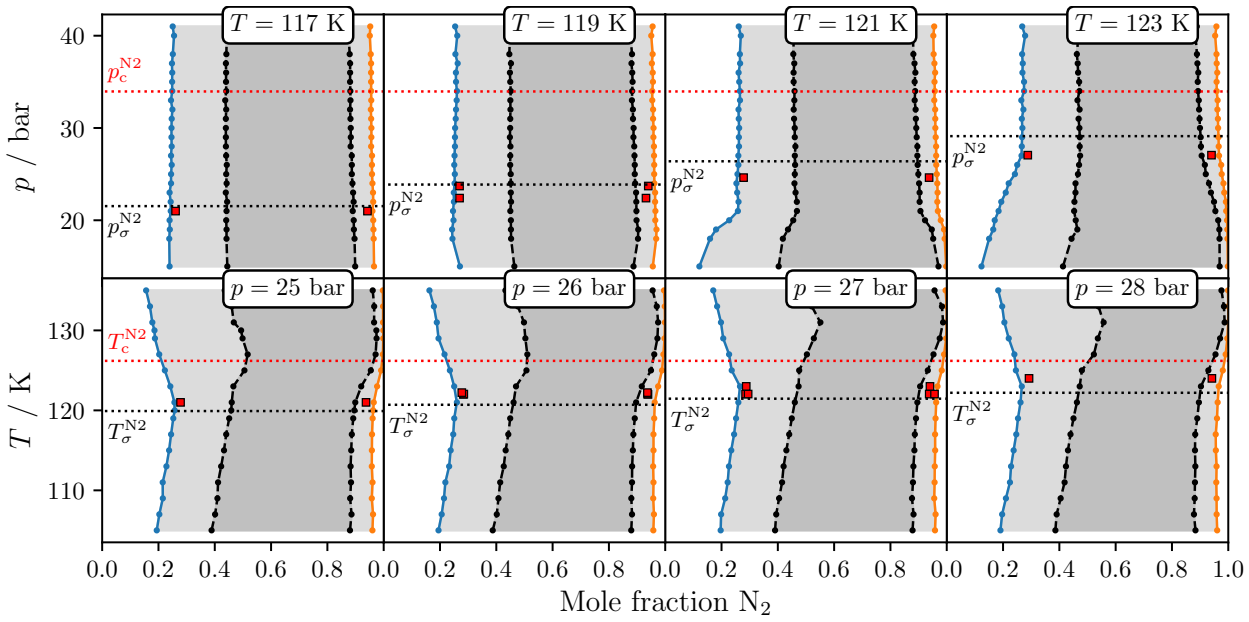

Figure 4: Selected LLE results in pressure-mole fraction and temperature-mole fraction phase diagrams of nitrogen + ethane. Critical point (T_c, p_c), boiling temperature T_σ and vapor pressure p_σ of nitrogen are included for orientation. Simulation results for binodal: phase I (blue) and phase II (orange); spinodal (black). Light gray: metastable region; dark gray: unstable region; red squares: experimental LLE data.[28–30,33,34]

sentation, the values are plotted over the number of experimental data points instead of temperature or pressure so that they are evenly distributed. A clear systematic bias can be seen for both phases. While the ethane-rich phase (I) is mostly underestimated with respect to the mole fraction, the nitrogen-rich phase (II) is overestimated by simulation. However, the average deviation for both phases is almost the same with about $\pm 0.025\,\mathrm{mol\,mol^{-1}}$. In phase I, the average deviation amounts to $-0.024\,\mathrm{mol\,mol^{-1}}$ and is slightly lower than in phase II with an average deviation of $+0.026\,\mathrm{mol\,mol^{-1}}$.

Vapor-Liquid-Liquid Equilibria

Since the UCEP marks the point below which all three types of phase equilibria can be presented simultaneously in one diagram, p-x and T-x diagrams are an expedient option to compare the simulation results with various datasets and thus allow to assess their physical plausibility by putting them in the larger context. Therefore, the simulation results are

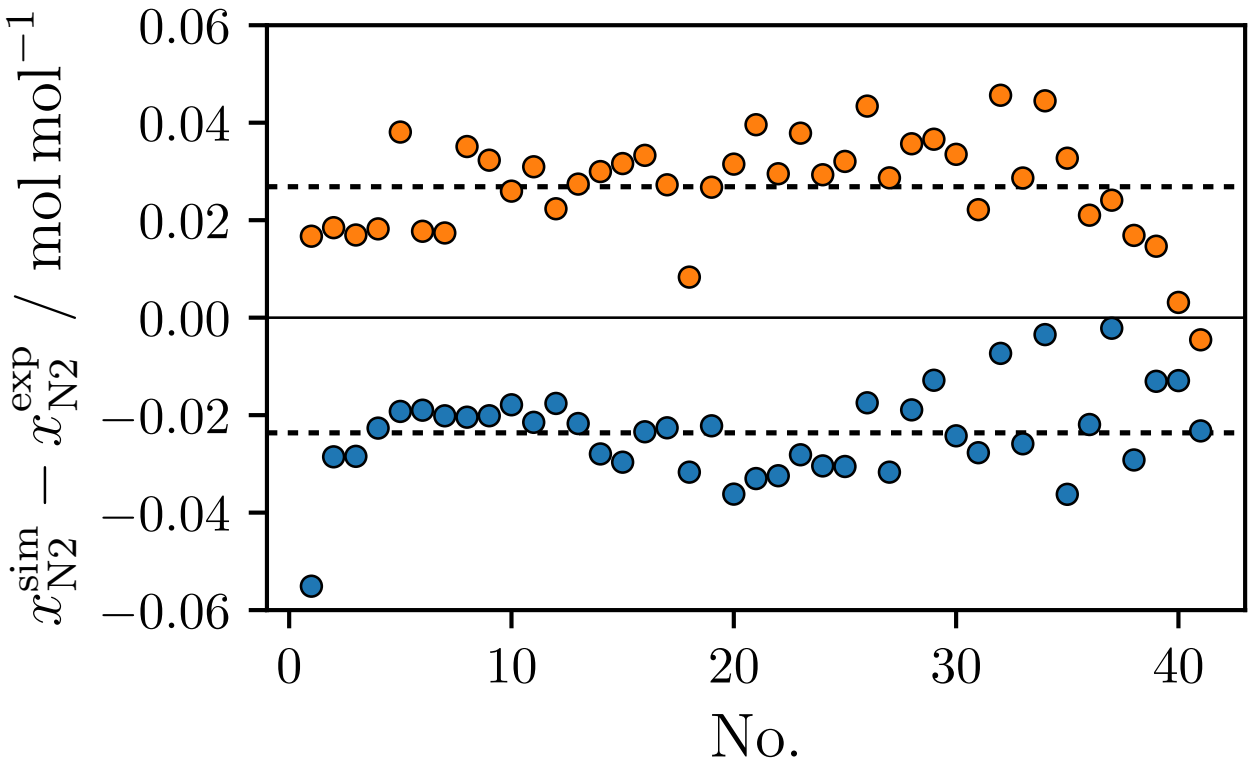

Figure 5: Deviation plot for the mole fraction of nitrogen under LLE conditions over the number of experimental data points; blue circles: phase I (ethane-rich); orange circles: phase II (nitrogen-rich); dashed line: average deviation.

displayed globally such that all available data for VLE, LLE and VLLE are included.

It should be noted that the VLE, LLE and VLLE from the GERG-2008 EOS were calculated with a newly developed algorithm[59] that was motivated by this work and is based on isochoric thermodynamics and the tracing approach.[60]

Figure 6 (top) shows the p-x diagram at $T = 125\,\mathrm{K}$. First, it can be noticed that the simulation results follow the binodal curve into the VLE in good agreement with the experimental data and EOS. This shows that the μ-x approach is in principle able to yield both LLE and VLE with somewhat better results for the liquid phase, which is not surprising, given the nature of excess Gibbs energy models. However, it was not the goal of this work to calculate VLE by means of adjusted g^{E} models. This can be done with far more sophisticated and reliable methods as shown with the additional GE simulations that were added inside the diagram.

Similar conclusions can be drawn for constant pressure. Figure 6 (center) shows the T-x diagram at $p = 24\,\mathrm{bar}$. Again, the simulation results follow the binodal curve, but an interesting observation can be made: The simulation data exhibit a bend in the direction of the respective coexistence line more often than not right at the experimental VLLE. This bend might indicate that a change occurs when moving from LLE to VLE, suggesting that there is a transition, namely the three-phase coexistence line.

By taking advantage of the bending location, the VLLE was obtained through additional vapor phase simulations in its direct vicinity and fulfilling Eq. (10) through the previously adjusted NRTL models. Figure 6 (bottom) shows the VLLE results at $p = 29\,\mathrm{bar}$. The VLLE was found to be at $T^{\mathrm{VLLE}} = 124.15\,\mathrm{K}$ and nitrogen mole fractions of $x_{\mathrm{N2}}^{\mathrm{L1}} = 0.269$, $x_{\mathrm{N2}}^{\mathrm{L2}} = 0.968$ and $y_{\mathrm{N2}}^{\mathrm{V}} = 0.9986\,\mathrm{mol\,mol^{-1}}$.

Thermodynamic Factor

The μ-x concept is not restrained to the chemical potential, but can also be applied on the basis of the thermodynamic factor Γ. With the knowledge of Γ as a function of mole fraction,

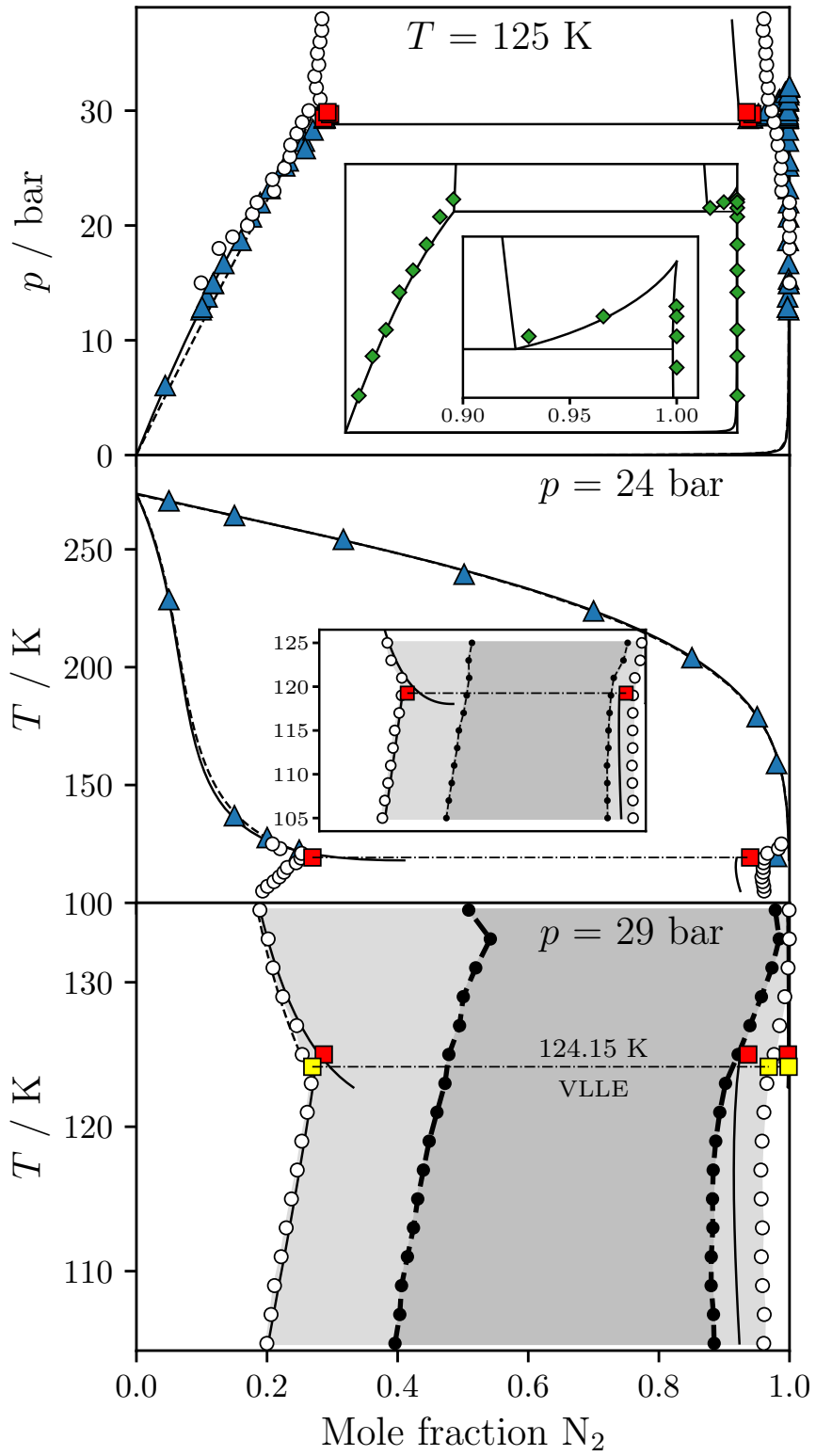

Figure 6: Pressure-mole fraction diagram at T=125 K including VLE simulations with the GE method (green diamonds) (top). Temperature-mole fraction diagram at p=24 bar with a zoom onthe LLE region (center). VLLE (yellow squares) for nitrogen + ethane at p = 29 bar (bottom). White circles: simulation data; solid line: GERG-2008 EOS;[25] dashed line: Peng-Robinson EOS; experimental data: VLE[33,61,62] (blue triangles), VLLE[30,33,34] (red squares).

it is possible to derive the phase equilibrium in the same way as with $\mu_i(x_i)$. Since KBI has recently been implemented in *ms2*,[39] the thermodynamic factor was accessed directly through simulation. This offers an alternative route for determining phase equilibria and is therefore beneficial to explore.

The values for Γ were calculated from KB integrals, which in turn were obtained from radial distribution functions (RDF). Fingerhut and Vrabec[55] used three types of RDF for the calculation of KBI: the standard RDF and two modifications – the corrected RDF as suggested by Ganguly and van der Vegt[63] (vdV) and a shifted version thereof (vdV + shf). Consequently, three versions of RDF were available for comparison.

An additional distinction has to be taken into account. Originally, KBI has been derived for the grand-canonical (μVT) ensemble[41] that is hardly applicable to dense liquid phases. KBI also contains an infinite integration limit $R \to \infty$ that cannot be reached with molecular simulation. However, with the formalism of Krüger et al.[64], it is possible to apply KBI to finite volume NVT ensemble data and to extrapolate the RDF to $R \to \infty$. Extrapolated RDF are denoted with "0" and are the ones that have shown the most promising results for phase equilibria in this work. Hence, the following results are presented on the basis of extrapolated RDF.

Figure 7 shows the simulation results for μ_i and Γ for all three types of RDF at $T = 121\,\mathrm{K}$ and $p = 30\,\mathrm{bar}$. For the purpose of comparison, the model adjusted to the chemical potential is regarded as the reference. It can be seen that the data based on RDF + vdV are in good agreement with that reference. In some cases, however, the combination RDF + vdV + shf yields better results. Thermodynamic factor data based on the standard RDF generally deviate most, which coincides with the conclusions of Fingerhut and Vrabec[55]. However, it can be noticed that the model adjustment to the thermodynamic factor is much more sensitive to inaccuracies than it is when adjusted to chemical potential data. For example, the thermodynamic factor based on the combination RDF + vdV + shf is mostly closer to the reference than the standard RDF. Therefore, the resulting LLE is expected to be

somewhat better. However, due to the sensitivity of the model adjustment, the opposite was observed.

The LLE results obtained from both μ_i and Γ are compared with experimental data in Figure 8 in a p-x diagram at $T = 121\,\mathrm{K}$. First, it should be noted that it is possible to calculate reasonable LLE from KBI-based thermodynamic factor data. Especially the data based on extrapolated RDF + vdV yield promising results. However, it is clear that with all three types of RDF the predicted miscibility gap is either too narrow or even vanishes. They are also far from being as smooth as the ones calculated from the chemical potential. As noted before, the adjustment of an excess Gibbs energy model was found to be much more sensitive with regard to the thermodynamic factor than to the chemical potential.

This might in part be due to the following reasons: While for μ_i two datasets (for each component one) are available to adjust the NRTL model, there is only one for Γ. This is because Γ involves the derivative of μ_i with respect to x_i and thus the number of data points reduces from two sets to only one for binary systems. Moreover, the adjustment is more prone to uncertainties because the derivative is involved. There is certainly potential to improve the results, but only so far as the simulation uncertainties with respect to KBI allow it. Overall, for the present mixture, LLE results from the chemical potential are considered more accurate.

Conclusion

We have extended the application range of a molecular nitrogen + ethane model from its original adjustment point at $T = 260\,\mathrm{K}$ under VLE conditions to temperatures and pressures around the three-phase VLLE where LLE are expected. The model was tested with the objective to see, whether and how well it is capable to predict LLE and VLLE given that only a single state-independent binary parameter ξ had been adjusted. Reasonable LLE results were obtained near the three-phase line that are in good agreement with experimental data

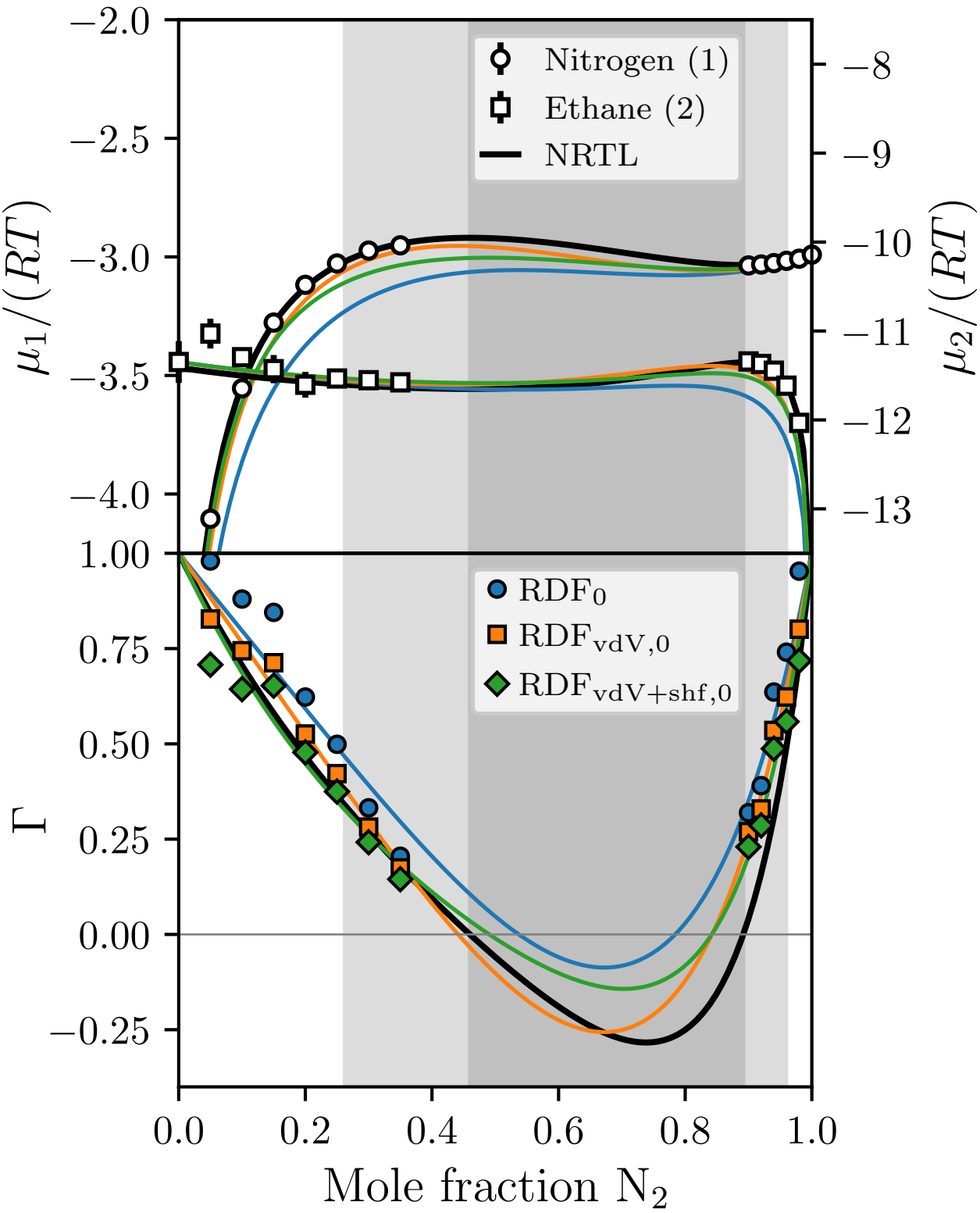

Figure 7: Chemical potentials (top) and thermodynamic factor (bottom) as a function of nitrogen mole fraction at $T = 121\,\mathrm{K}$ and $p = 30\,\mathrm{bar}$. Comparison between μ_i and Γ, calculated from KBI on the basis of different RDF. Solid lines: NRTL model adjusted to different datasets. Light gray: metastable region; dark gray: unstable region.

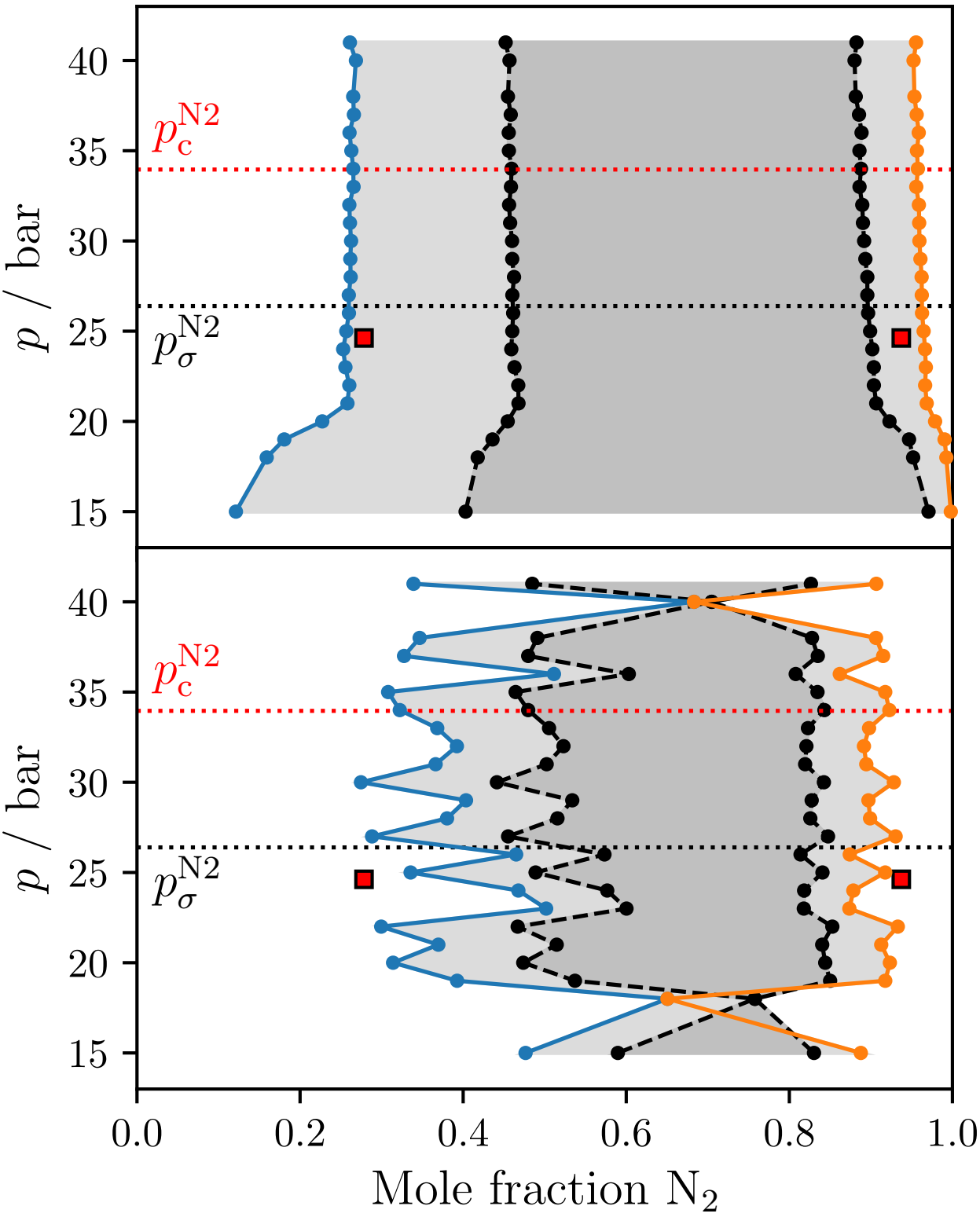

Figure 8: Comparison between μ_i (top) and Γ (bottom) based LLE in the p-x diagram at $T = 121\,\mathrm{K}$. Thermodynamic factor calculated from KBI on the basis of extrapolated RDF+vdV. Simulation results for the binodal: phase I (blue) and phase II (orange); spinodals (black). Light gray: metastable region; dark gray: unstable region; red squares: experimental LLE data.[34]

and the GERG-2008 EOS. As a Type III system, the mixture nitrogen + ethane exhibits remarkable shape transitions of the phase envelope and a large miscibility gap which was successfully predicted. Over the course of this work, we have faced the problem of glancing intersections when utilizing μ-p based concepts, e.g. the grand equilibrium method, for this specific mixture at low temperatures. While the GE method is an efficient approach to sample VLE, it struggles with high-density state points, i.e. LLE, or close to the critical point. This is likely due to glancing intersections, where small uncertainties of the simulation data can lead to large intersection ranges. Therefore, we changed gears and applied the μ-x concept, which has led to sound LLE results with the additional advantage of being flexible regarding the constant variable T or p. It does come with the disadvantage that a linear function can no longer be used for approximating μ_i, but an excess Gibbs energy model is needed with an adjustment procedure, which is susceptible to errors. However, the results have shown that the μ-x concept can yield physically and thermodynamically sound results for different temperatures and pressures. The average deviation was very similar for both phases and amounted to a value of $\pm 0.025\,\mathrm{mol\,mol^{-1}}$. Additional vapor phase simulations allowed to determine the VLLE by taking advantage of the binodal curvature and its bending location. LLE were also investigated based on the thermodynamic factor obtained from Kirkwood-Buff integration. Beside the chemical potential, the thermodynamic factor is another property from which phase equilibria can be determined, among other applications. Depending on the type of RDF and whether it was extrapolated to the thermodynamic limit or not, different results were observed. Extrapolated Kirkwood-Buff integrals based on RDF that were corrected according to the method of Ganguly and van der Vegt [63] showed the most promising binodal curves, but overall the LLE from the thermodynamic factor could only yield unsatisfactory results compared to the ones resting on the chemical potential.

Acknowledgement

This work was supported by the Deutsche Forschungsgemeinschaft (DFG) under grant no. VR 6/16. Equilibrium molecular dynamics simulations were performed on Cray's CS500 system Noctua 1 and the OCuLUS cluster at the Paderborn Center for Parallel Computing (PC2), the HPE Apollo system Hawk at the High Performance Computing Centre Stuttgart (HLRS) and the SuperMUC system at the Leibniz-Rechenzentrum (LRZ), contributing to the project MMHBF2.

Supporting Information Available

See the supporting information for further technical details, diagrams of the LLE results and tabulated numerical simulation values in this study.

References

(1) Romig, K.; Hanley, H. Calculation of phase equilibria in nitrogen-ethane mixtures by extended corresponding states. *Cryogenics* **1986**, *26*, 33–38.

(2) van Konynenburg, P. H.; Scott, R. L. Critical lines and phase equilibria in binary van der Waals mixtures. *Philos. Trans. R. Soc. London, Ser. A* **1980**, *298*, 495–540.

(3) Bolz, A.; Deiters, U. K.; Peters, C. J.; de Loos, T. W. Nomenclature for phase diagrams with particular reference to vapour–liquid and liquid–liquid equilibria (Technical report). *Pure Appl. Chem.* **1998**, *70*, 2233–2258.

(4) Cox, A. L.; Vries, T. D. The Solubility of Solid Ethane, Ethylene, and Propylene in Liquid Nitrogen and Oxygen. *J. Phys. Colloid Chem.* **1950**, *54*, 665–670.

(5) Eakin, B. E.; Ellington, R.; Gami, D. *Physical-chemical properties of ethane-nitrogen mixtures*; Institute of Gas Technology, 1955; pp 1–41.

(6) Ellington, R.; Eakin, B.; Parent, J.; Gami, D.; Bloomer, O. Vapor–liquid phase equilibria in the binary systems of methane, ethane and nitrogen. *Thermodynamic and Transport Properties of Gases, Liquids and Solids* **1959**, 180–194.

(7) Cheung, H.; Wang, D. I.-J. Solubility of Volatile Gases in Hydrocarbon Solvents at Cryogenic Temperatures. *Ind. Eng. Chem. Fundam.* **1964**, *3*, 355–361.

(8) Rozhnov, M.; Kozya, V.; Zhdanov, V. Phase ratios in twocomponent systems of C1-3 hydrocarbons and nitrogen. *Khim. Promst. (Moscow)* **1988**, *11*, 674–675.

(9) Brown, T.; Sloan, E.; Kidnay, A. Vapor-liquid equilibria in the nitrogen + carbon dioxide + ethane system. *Fluid Phase Equilib.* **1989**, *51*, 299–313.

(10) Raabe, G.; Janisch, J.; Koehler, J. Experimental studies of phase equilibria in mixtures relevant for the description of natural gases. *Fluid Phase Equilib.* **2001**, *185*, 199–208.

(11) Janisch, J.; Raabe, G.; Köhler, J. Vapor-Liquid Equilibria and Saturated Liquid Densities in Binary Mixtures of Nitrogen, Methane, and Ethane and Their Correlation Using the VTPR and PSRK GCEOS. *J. Chem. Eng. Data* **2007**, *52*, 1897–1903.

(12) Wisotzki, K. D.; Schneider, G. M. Fluid Phase Equilibria of the Binary Systems N2 + Ethane and N2 + Pentane Between 88 K and 313 K and at Pressures up to 200 MPa. *Ber. Bunsenges. Phys. Chem.* **1985**, *89*, 21–25.

(13) Llave, F. M.; Luks, K. D.; Kohn, J. P. Three-phase liquid-liquid-vapor equilibria in the binary systems nitrogen + ethane and nitrogen + propane. *J. Chem. Eng. Data* **1985**, *30*, 435–438.

(14) Yun, S. Experimental and Thermodynamical studies of the phase equilibria for carbon dioxide in liquefied natural gas components at 77-219 K. Ph.D. thesis, University of Southampton, 1988.

(15) Raabe, G. *Dampf-Flüssig-Phasengleichgewichte bei tiefen Temperaturen*; Shaker: Aachen, 2002; pp 76–85.

(16) Bell, I. H.; Jäger, A. Calculation of critical points from Helmholtz-energy-explicit mixture models. *Fluid Phase Equilib.* **2017**, *433*, 159–173.

(17) Vrabec, J.; Stoll, J.; Hasse, H. A Set of Molecular Models for Symmetric Quadrupolar Fluids. *J. Phys. Chem. B* **2001**, *105*, 12126–12133.

(18) Stoll, J.; Vrabec, J.; Hasse, H. Vapor–liquid equilibria of mixtures containing nitrogen, oxygen, carbon dioxide, and ethane. *AlChE J.* **2003**, *49*, 2187–2198.

(19) Kronome, G.; Szalai, I.; Wendland, M.; Fischer, J. Extension of the NpT + test particle method for the calculation of phase equilibria of nitrogen + ethane. *J. Mol. Liq.* **2000**, *85*, 237–247.

(20) Carrero-Mantilla, J.; Llano-Restrepo, M. Vapor–liquid equilibria of the binary mixtures nitrogen + methane, nitrogen + ethane and nitrogen + carbon dioxide, and the ternary mixture nitrogen + methane + ethane from Gibbs-ensemble molecular simulation. *Fluid Phase Equilib.* **2003**, *208*, 155–169.

(21) Guo, M.; Li, Y.; Li, Z.; Lu, J. Molecular simulation of liquid-liquid equilibria for Lennard-Jones fluids. *Fluid Phase Equilib.* **1994**, *98*, 129–139.

(22) Sadus, R. J. Molecular simulation of the liquid-liquid equilibria of binary mixtures containing dipolar and non-polar components interacting via the Keesom potential. *Mol. Phys.* **1996**, *89*, 1187–1194.

(23) Gordon, P. A.; Glandt, E. D. Liquid–liquid equilibrium for fluids confined within random porous materials. *J. Chem. Phys.* **1996**, *105*, 4257–4264.

(24) Wang, X.; Gu, X.; Murad, S. Molecular dynamics simulations of liquid-liquid phase

equilibrium of ternary methanol/water/hydrocarbon mixtures. *Fluid Phase Equilib.* **2018**, *470*, 109–119.

(25) Kunz, O.; Wagner, W. The GERG-2008 Wide-Range Equation of State for Natural Gases and Other Mixtures: An Expansion of GERG-2004. *J. Chem. Eng. Data* **2012**, *57*, 3032–3091.

(26) Peng, D.-Y.; Robinson, D. B. A New Two-Constant Equation of State. *Ind. Eng. Chem. Fundam.* **1976**, *15*, 59–64.

(27) Grausø, L.; Fredenslund, A.; Mollerup, J. Vapour-liquid equilibrium data for the systems C2H6 + N2, C2H4 + N2, C3H8 + N2, and C3H6 + N2. *Fluid Phase Equilib.* **1977**, *1*, 13–26.

(28) Chang, S.-D.; Lu, B. C. Vapor-liquid equilibriums in the nitrogen-methane-ethane system. *Chemical Engineering Progress Symposium Series* **1967**, *63*, 18–27.

(29) Lu, B.; Chang, S.; Elshayal, I.; Yu, P.; Gravelle, D.; Poon, D. Low temperature phase equilibria of natural gas components. Proc. 1st Int. Conf. Calorimetry and Thermodynamics, Warsaw. 1969; p 775.

(30) Yu, P.; Elshayal, I. M.; Lu, B. C.-Y. Liquid-liquid-vapor equilibria in the nitrogen-methane-ethane system. *Can. J. Chem. Eng.* **1969**, *47*, 495–498.

(31) Wilson, G. M. Vapor–liquid equilibria of nitrogen, methane, ethane, and propane binary mixtures at LNG temperatures from total pressure measurements. *Adv. Cryog. Eng.* **1975**, *20*, 164–171.

(32) Gasem, K.; Hiza, M.; Kidnay, A. Phase behavior in the nitrogen + ethylene system from 120 to 200 K. *Fluid Phase Equilib.* **1981**, *6*, 181–189.

(33) Kremer, H.; Knapp, H. Three-phase conditions are predictable. *Hydrocarbon Process.* **1983**, *62*, 79–83.

(34) Kohn, J. P.; Llave, F.; Luks, K. D. *Liquid-liquid-vapor Equilibria in Cryogenic LNG Mixtures, Phase IV: Nitrogen Rich Systems*; Gas Processors Association, 1984.

(35) Guedes, H. J.; Zollweg, J. A.; Filipe, E. J.; Martins, L. F.; Calado, J. C. Thermodynamics of liquid (nitrogen + ethane). *J. Chem. Thermodyn.* **2002**, *34*, 669–678.

(36) Deublein, S.; Eckl, B.; Stoll, J.; Lishchuk, S. V.; Guevara-Carrion, G.; Glass, C. W.; Merker, T.; Bernreuther, M.; Hasse, H.; Vrabec, J. ms2: A molecular simulation tool for thermodynamic properties. *Comput. Phys. Commun.* **2011**, *182*, 2350–2367.

(37) Glass, C. W.; Reiser, S.; Rutkai, G.; Deublein, S.; Köster, A.; Guevara-Carrion, G.; Wafai, A.; Horsch, M.; Bernreuther, M.; Windmann, T.; Hasse, H.; Vrabec, J. ms2: A molecular simulation tool for thermodynamic properties, new version release. *Comput. Phys. Commun.* **2014**, *185*, 3302–3306.

(38) Rutkai, G.; Köster, A.; Guevara-Carrion, G.; Janzen, T.; Schappals, M.; Glass, C. W.; Bernreuther, M.; Wafai, A.; Stephan, S.; Kohns, M.; Reiser, S.; Deublein, S.; Horsch, M.; Hasse, H.; Vrabec, J. ms2: A molecular simulation tool for thermodynamic properties, release 3.0. *Comput. Phys. Commun.* **2017**, *221*, 343–351.

(39) Fingerhut, R.; Guevara-Carrion, G.; Nitzke, I.; Saric, D.; Marx, J.; Langenbach, K.; Prokopev, S.; Celný, D.; Bernreuther, M.; Stephan, S.; Kohns, M.; Hasse, H.; Vrabec, J. ms2: A molecular simulation tool for thermodynamic properties, release 4.0. *Comput. Phys. Commun.* **2021**, *262*, 107860.

(40) Lustig, R. Angle-average for the powers of the distance between two separated vectors. *Mol. Phys.* **1988**, *65*, 175–179.

(41) Kirkwood, J. G.; Buff, F. P. The Statistical Mechanical Theory of Solutions. I. *J. Chem. Phys.* **1951**, *19*, 774–777.

(42) Widom, B. Some Topics in the Theory of Fluids. *J. Chem. Phys.* **1963**, *39*, 2808–2812.

(43) Lorentz, H. A. Über die Anwendung des Satzes vom Virial in der kinetischen Theorie der Gase. *Ann. Phys.* **1881**, *248*, 127–136.

(44) Berthelot, D. Sur le mélange des gaz. *Comptes Rendus Hebdomadaires des Séances de l'Académie des Sciences* **1898**, *126*, 1703–1706.

(45) Panagiotopoulos, A. Z. Direct determination of phase coexistence properties of fluids by Monte Carlo simulation in a new ensemble. *Mol. Phys.* **1987**, *61*, 813–826.

(46) Panagiotopoulos, A. Exact calculations of fluid-phase equilibria by Monte Carlo simulation in a new statistical ensemble. *Int. J. Thermophys.* **1989**, *10*, 447–457.

(47) Kofke, D. A. Gibbs-Duhem integration: a new method for direct evaluation of phase coexistence by molecular simulation. *Mol. Phys.* **1993**, *78*, 1331–1336.

(48) Kofke, D. A. Direct evaluation of phase coexistence by molecular simulation via integration along the saturation line. *J. Chem. Phys.* **1993**, *98*, 4149–4162.

(49) Ungerer, P.; Boutin, A.; Fuchs, A. H. Direct calculation of bubble points by Monte Carlo simulation. *Mol. Phys.* **1999**, *97*, 523–539.

(50) BODA, D.; Kristóf, T.; Liszi, J.; Szalai, I. A new simulation method for the determination of phase equilibria in mixtures in the grand canonical ensemble. *Mol. Phys.* **2001**, *99*, 2011–2022.

(51) Möller, D.; Fischer, J. Vapour liquid equilibrium of a pure fluid from test particle method in combination with NpT molecular dynamics simulations. *Mol. Phys.* **1990**, *69*, 463–473.

(52) Vrabec, J.; Fischer, J. Vapour liquid equilibria of mixtures from the NpT plus test particle method. *Mol. Phys.* **1995**, *85*, 781–792.

(53) Vrabec, J.; Hasse, H. Grand Equilibrium: vapour-liquid equilibria by a new molecular simulation method. *Mol. Phys.* **2002**, *100*, 3375–3383.

(54) Renon, H.; Prausnitz, J. M. Local compositions in thermodynamic excess functions for liquid mixtures. *AlChE J.* **1968**, *14*, 135–144.

(55) Fingerhut, R.; Vrabec, J. Kirkwood-Buff integration: A promising route to entropic properties? *Fluid Phase Equilib.* **2019**, *485*, 270–281.

(56) Gupta, M. K.; Gardner, G. C.; Hegarty, M. J.; Kidnay, A. J. Liquid-vapor equilibriums for the N2 + CH4 + C2H6 system from 260 to 280 K. *J. Chem. Eng. Data* **1980**, *25*, 313–318.

(57) Zeck, S.; Knapp, H. Vapor-liquid and vapor-liquid-liquid phase equilibria for binary and ternary systems for nitrogen, ethane and methanol: Experiment and data reduction. *Fluid Phase Equilib.* **1986**, *25*, 303–322.

(58) Stryjek, R.; Chappelear, P. S.; Kobayashi, R. Low-temperature vapor-liquid equilibriums of nitrogen-methane system. *J. Chem. Eng. Data* **1974**, *19*, 334–339.

(59) Bell, I. H.; Deiters, U. K.; Jäger, A. Algorithm to Identify Vapor–Liquid–Liquid Equilibria of Binary Mixtures from Vapor–Liquid Equilibria. *Industrial & Engineering Chemistry Research* **2022**, *0*, 0.

(60) Bell, I. H.; Deiters, U. K. On the construction of binary mixture p-x and T-x diagrams from isochoric thermodynamics. *AlChE J.* **2018**, *64*, 2745–2757.

(61) Trappehl, G.; Knapp, H. Vapour-liquid equilibria in the ternary mixtures N2+CH4+C2H6 and N2+C2H6+C3H8. *Cryogenics* **1987**, *27*, 696–716.

(62) Raabe, G.; Köhler, J. Phase equilibria in the system nitrogen-ethane and their prediction using cubic equations of state with different types of mixing rules. *Fluid Phase Equilib.* **2004**, *222-223*, 3–9.

(63) Ganguly, P.; van der Vegt, N. F. A. Convergence of Sampling Kirkwood–Buff Integrals

of Aqueous Solutions with Molecular Dynamics Simulations. *J. Chem. Theory Comput.* **2013**, *9*, 1347–1355.

(64) Krüger, P.; Schnell, S. K.; Bedeaux, D.; Kjelstrup, S.; Vlugt, T. J. H.; Simon, J.-M. Kirkwood-Buff Integrals for Finite Volumes. *J. Phys. Chem. Lett.* **2013**, *4*, 235–238.

TOC Graphic

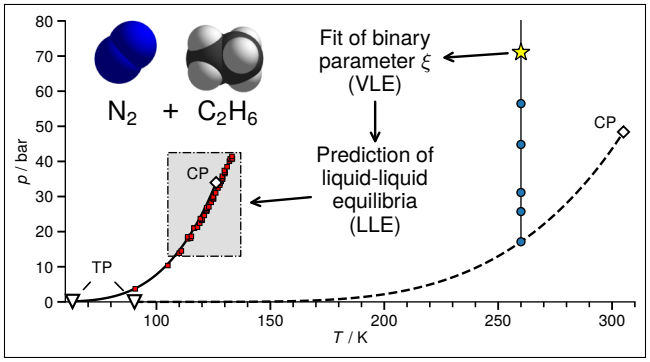
80
70
60
50
40
30
20
10
0
p / bar
100
150
200
250
300
T / K
N2 + C2H6
CP
TP
CP
Fit of binary parameter ξ (VLE)
Prediction of liquid-liquid equilibria (LLE)

Supporting Information: Vapor-Liquid-Liquid Equilibria of Nitrogen + Ethane by Molecular Simulation

Ivan Antolović and Jadran Vrabec*

Thermodynamics and Process Engineering, Technical University Berlin, 10587 Berlin, Germany

E-mail: vrabec@tu-berlin.de

Phone: +49 30 314 22755

Contents

1 Technical Details of Molecular Simulations

1.1 VLE Simulations

VLE simulations were carried out in two steps: (1) liquid run and (2) vapor run, following the grand equilibrium method developed by Vrabec and Hasse[S1]. The liquid run was sampled with Molecular Dynamics (MD) simulations in the NpT ensemble with $N = 1372$ molecules and a total of $3.2 \cdot 10^6$ production steps. Newton's equations of motion were solved with a fifth-order Gear predictor-corrector numerical integrator and an integration time step of 1 fs. The simulations were carried out on the HPE Apollo (Hawk) system at the High-Performance Computing Center Stuttgart (HLRS). The gas run was then sampled with MC simulations in the pseudo-μVT ensemble with $N = 500$ molecules and a total of $2 \cdot 10^5$ production steps. The simulations were carried out on the OCuLUS cluster at the Paderborn Center for Parallel Computing (PC2).

1.2 LLE Simulations

LLE simulations were conducted in two consecutive steps: (1) Monte Carlo (MC) simulations in the NpT ensemble to obtain initial densities and (2) MD simulations in the NVT ensemble to obtain the chemical potentials as well as the thermodynamic factor through Kirkwood-Buff integrals (KBI).[S2] The possibility of using KBI has recently been implemented into the massively-parallel molecular simulation tool *ms2*.[S3–S6] While KBI can be invoked both for MC or MD simulations, it is currently only applicable to the NVT ensemble in *ms2*.[S7] Hence, preliminary simulations were carried out, to determine the density needed for the NVT simulations. For all MC and MD simulations, the cutoff radius was set to 14 Å.

1. **Density:** Monte-Carlo simulations were carried out as preliminary simulations in the NpT ensemble over $7 \cdot 10^4$ cycles for a system of 864 molecules. The density simulations were carried out on the OCuLUS cluster and the Cray CS500 system (Noctua 1) at the Paderborn Center for Parallel Computing (PC2).

2. **Chemical Potential and Thermodynamic Factor:** After calculating the density, MD simulations in the NVT ensemble were carried out. The number of molecules was set to $N = 4000$ with $1.5 \cdot 10^7$ production time steps. Equilibration was set to $3 \cdot 10^5$ time steps preceded by 10 MC relaxation loops for pre-equilibration. Chemical potentials μ_i were sampled with Widom's test particle insertion method[S8] with 4000 test insertions per time step. The thermodynamic factor was calculated from KBI[S2] with the RDF being sampled each time step as well. The simulations were carried out on the HPE Apollo (Hawk) system at the High-Performance Computing Center Stuttgart (HLRS) and the SuperMUC system at the Leibniz-Rechenzentrum (LRZ).

1.3 VLLE Simulations

Additional vapor phase simulations were conducted to obtain the VLLE. Since the nitrogen mole fraction of the vapor phase was expected to be very close to unity ($x_{\mathrm{N2}}^{\mathrm{VLLE}} \approx 0.999\,\mathrm{mol\,mol^{-1}}$), the number of molecules was increased from $N = 500$ to $N = 2000$. The vapor phase was sampled with MC simulations in the NpT ensemble with $1 \cdot 10^4$ NVT equilibration steps, $5 \cdot 10^4$ NpT equilibration steps and $1 \cdot 10^6$ production cycles. Chemical potentials μ_i were sampled with Widom's test particle insertion method[S8] with 3000 test insertions per cycle. The simulations were carried out on the OCuLUS cluster at the Paderborn Center for Parallel Computing (PC2).

2 Calculating Phase Equilibria

2.1 Example of μ-p Concept

Figure S1 shows the μ-p diagram for nitrogen and ethane at 105 K. Next to the temperature, the mole fraction $x_{\mathrm{N2}}^{\mathrm{I}} = 0.20\,\mathrm{mol\,mol^{-1}}$ of the ethane-rich phase was specified. Since both phases are liquid and thus little compressible, the isotherms can be approximated by linear

functions. LLE were obtained by varying the mole fraction x_i^{II}, while keeping x_i^{I} constant, so that the isotherms intersect at the same pressure.

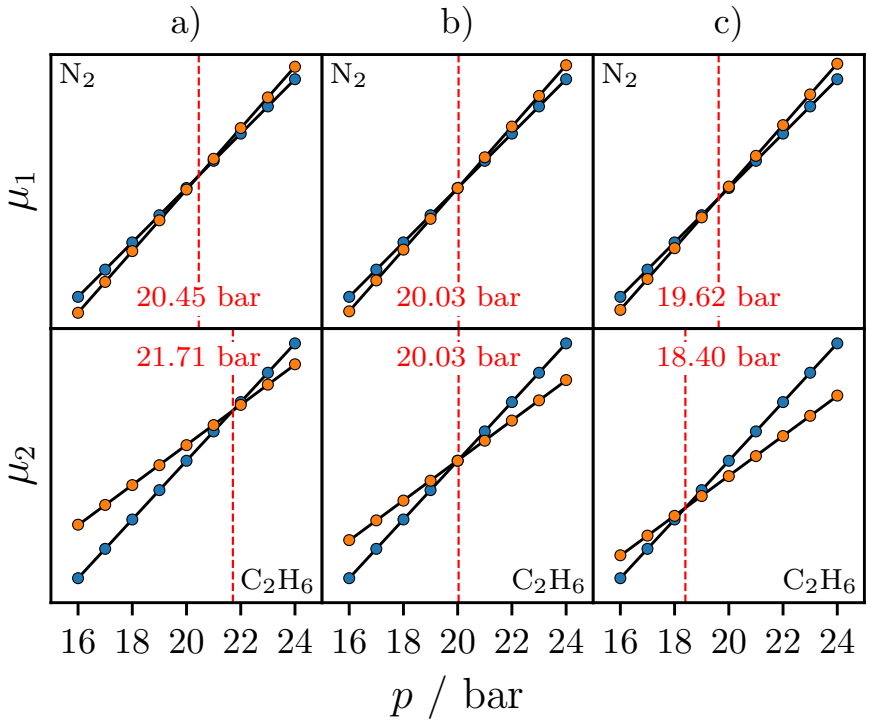

Figure S1: Chemical potentials as a function of pressure at T=105 K. Data points generated by REFPROP[S9] on the basis of GERG-2008,[S10] blue circles: ethane-rich phase (I) at $x_{\mathrm{N2}}^{\mathrm{I}} = 0.2\,\mathrm{mol\,mol^{-1}}$; orange circles: nitrogen-rich phase (II) at a) $x_{\mathrm{N2}}^{\mathrm{II}} = 0.9255\,\mathrm{mol\,mol^{-1}}$, b) $x_{\mathrm{N2}}^{\mathrm{II}} = 0.9260\,\mathrm{mol\,mol^{-1}}$, c) $x_{\mathrm{N2}}^{\mathrm{II}} = 0.9265\,\mathrm{mol\,mol^{-1}}$; solid line: adjusted linear model.

2.2 Example of μ-x Concept

Figure S2 shows the μ_i-x and the g^{mix}-x diagrams for nitrogen + ethane again at 105 K. To maintain comparability, the pressure was set to $p_\sigma = 20.034\,\mathrm{bar}$, which is the average value of the two very similar solutions from the μ-p concept. The phase equilibrium conditions are fulfilled at the binodal, which is at the outer limits of the light gray area that indicates the metastable region.

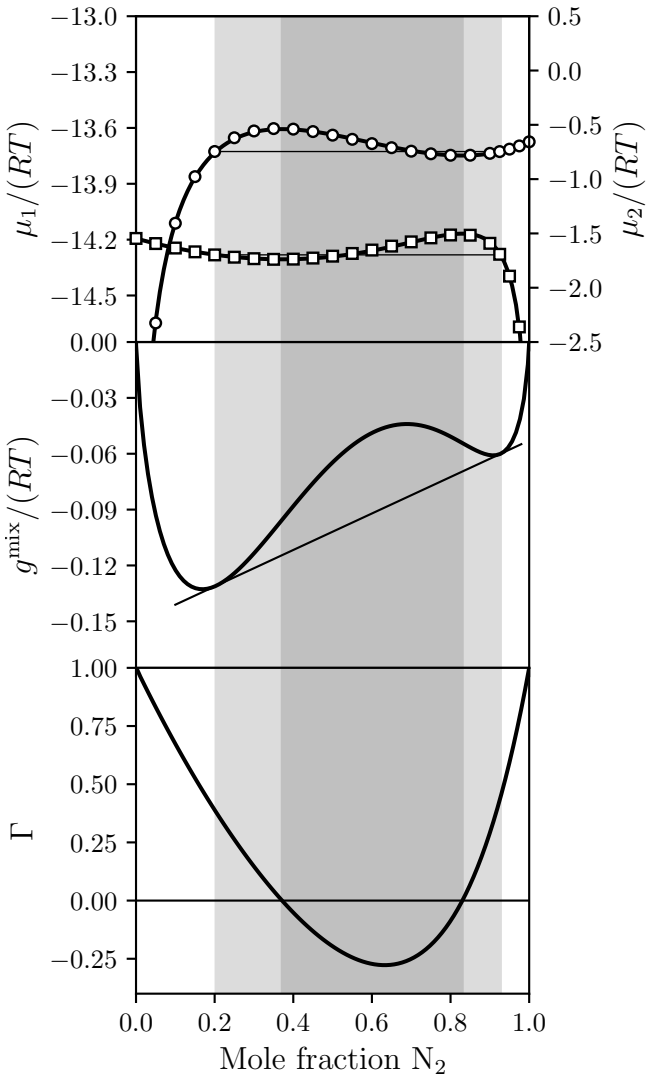

Figure S2: Chemical potentials (top), Gibbs energy of mixing (center) and thermodynamic factor (bottom) of nitrogen + ethane as a function of nitrogen mole fraction x_{N2} with a liquid-liquid equilibrium at $T = 105\,\mathrm{K}$ and $p = 20.03\,\mathrm{bar}$. Data points were generated by REFPROP[S9] on the basis of the GERG-2008 EOS;[S10] circles: nitrogen, squares: ethane, solid line: adjusted NRTL model. Light gray: metastable region; dark gray: unstable region.

2.3 Comparison of the μ-p and μ-x Concepts

The numerical results obtained with both concepts are listed in Table S1. Considering the uncertainties that inevitably occur during model approximation, the results are almost identical for $T = 105\,\mathrm{K}$ and $p = 20.034\,\mathrm{bar}$. Even though the underlying approach differs – "finding intersections" vs. "finding contact points of tangent line" – both concepts are thermodynamically consistent and capable of yielding the same miscibility gap, provided

that the chemical potentials are described correctly. With respect to accuracy, the linear approximation of the chemical potential $\mu_i(p)$ in the liquid phase is considered to be more accurate than the more laborious approximation of $\mu_i(x_i)$, which relies on the choice of a suitable excess Gibbs energy model.

Table S1: LLE results obtained from the μ-p and μ-x concepts at $T = 105\,\mathrm{K}$.

	$x_{\mathrm{N2}}/\mathrm{mol\,mol^{-1}}$			
Concept	Phase I	Phase II	p^I/bar	p^{II}/bar
μ-p	0.2000	0.9260	20.0334	20.0343
μ-x	0.2031	0.9272	20.0339	20.0339

However, for phase equilibria close to the critical point or in the LLE region, the μ-p concept is more prone to uncertainties due to glancing intersections, which may lead to imprecise or even no phase equilibria. The occurrence of glancing intersections is described in more detail below. Another drawback of μ-p-based approaches is their inability to yield phase equilibria at constant pressure, i.e. to generate T-x diagrams. Both disadvantages can be overcome with the μ-x concept, which is not associated with glancing intersections and is flexible in its application to either p-x or T-x diagrams. In addition, it allows for the prediction of the spinodal curves and the calculation of the thermodynamic factor, which is an important property for the transformation between Fick and Maxwell-Stefan diffusion coefficients.[S11]

2.4 Glancing Intersections

Approaches that are based on the μ-p concept can face the problem of glancing intersections when calculating LLE. If both phases are liquid, the slopes of the isotherms become so similar that even minor uncertainties of the simulation data can lead to large intersection ranges, which make an accurate calculation of the phase equilibrium virtually impossible. Figure S3 shows the chemical potential of nitrogen and ethane along the isotherm $T = 121\,\mathrm{K}$ to illustrate the problem. Even though the chemical potential of nitrogen can be reason-

ably well approximated by a linear function, the similarity of the slopes of both isotherms in combination with the simulation uncertainties leads to a wide glancing intersection with an uncertainty of $\delta p = 10.33\,\mathrm{bar}$ rather than a well-defined intersection point. This applies even more to the chemical potential of ethane. The isotherm in the nitrogen-rich phase is almost perfectly linear, but since the chemical potential data in the ethane-rich phase are scattered according to their large statistical uncertainty, an even larger glancing intersection uncertainty of $\delta p = 20.67\,\mathrm{bar}$ was obtained. As a result, the phase equilibrium cannot be accurately determined, but at most roughly estimated. The GE method uses a more sophisticated implementation of the μ-p concept, but nevertheless the core problem of glancing intersections remains.

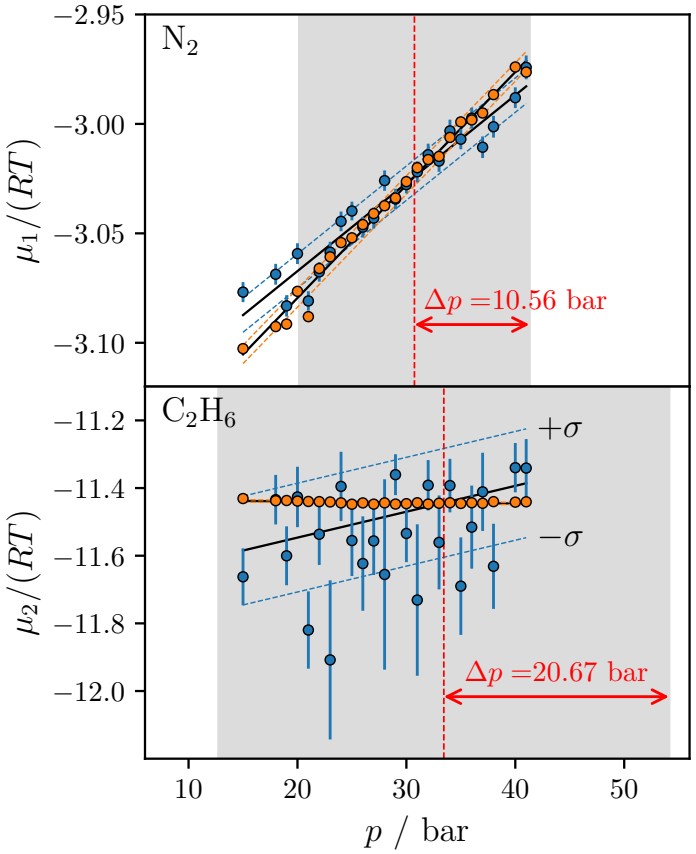

Figure S3: Glancing intersection: Chemical potentials of nitrogen and ethane as a function of pressure at $T = 121\,\mathrm{K}$. Similar slopes and simulation uncertainties lead to ill-defined intersections. Red dashed lines indicate intersection points, gray area: glancing intersection. Constant nitrogen mole fractions: $x_{\mathrm{N2}} = 0.25\,\mathrm{mol\,mol^{-1}}$ (blue circles); $x_{\mathrm{N2}} = 0.94\,\mathrm{mol\,mol^{-1}}$ (orange circles); solid line: linear fit; dashed line: root mean square deviation.

Figure S4 shows the results for the chemical potential at the same temperature of $T = 121\,\mathrm{K}$ as before and a pressure of $p = 29\,\mathrm{bar}$. The simulation points were chosen to be outside of the unstable region to rule out physically meaningless state points. Both $\mu_i(x_i)$ curves were then simultaneously approximated with a suitable activity coefficient model. Several models were tested beforehand, namely the Nonrandom Two Liquid Theory (NRTL), the modified Wilson model[S12,S13] and the Universal Quasi-Chemical Theory (UNIQUAC).[S14] Since the NRTL model led to the best results in terms of adjustment accuracy, it was chosen for all subsequent calculations.

By looking at the chemical potential of both components in the two coexisting liquid phases, it can be seen that three of the four simulation datasets are statistically sound and only the chemical potential of ethane in the ethane-rich phase scatters significantly. Despite this scatter, the three sound sets of data are sufficient to compensate for the uncertainty of the fourth and to ensure a viable NRTL model adjustment. This can be explained by the Gibbs-Duhem equation, which states that the chemical potentials in mixtures at constant temperature and pressure are not independent from each other. With the adjusted NRTL model, both the binodal and the spinodal can be calculated, yielding adequate LLE results.

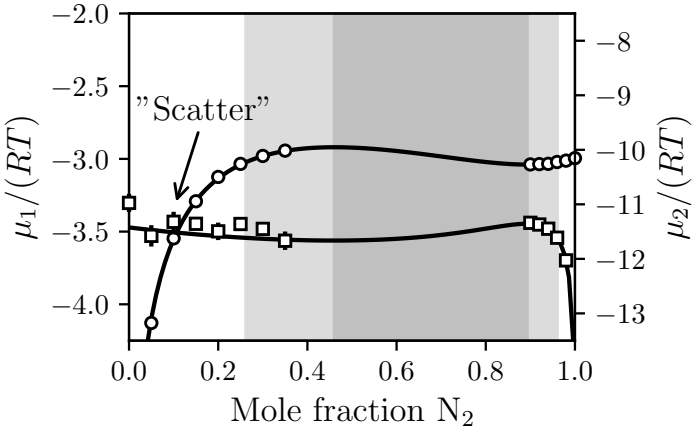

Figure S4: Chemical potentials as a function of nitrogen mole fraction at $T = 121\,\mathrm{K}$ and $p = 29\,\mathrm{bar}$; solid line: adjusted NRTL model. The scattered chemical potential data of ethane in the ethane-rich phase are compensated by the remaining data. Circles: nitrogen, squares: ethane, solid line: adjusted NRTL model. Light gray: metastable region; dark gray: unstable region.

2.5 Three-Phase Equilibria

The three-phase equilibrium can be calculated with both the μ-p and μ-x concept. Figure S5 (left) shows the μ-p diagrams for nitrogen and ethane at $T = 133.15\,\mathrm{K}$ and (right) the μ-x and g^{mix}-x diagrams at $p = 40.9\,\mathrm{bar}$. It is clear that both approaches yield the same results for the VLLE.

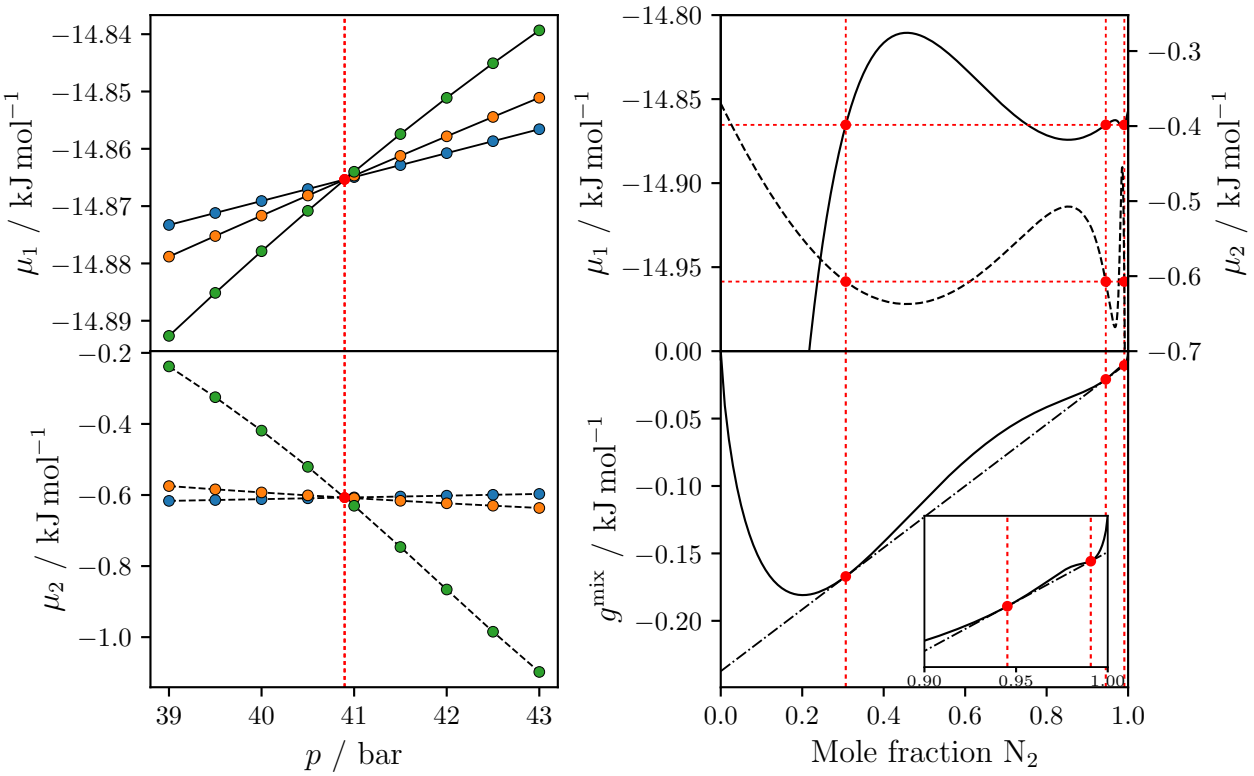

Figure S5: Calculation of VLLE through the μ-p and μ-x concepts. The intersection of the three isotherms (left) is equivalent to the touching points of the tangent in the g^{mix}-x diagram (bottom right) where the equality of chemical potentials is reached for both components (top right). Data were generated by REFPROP[S9] on the basis of the GERG-2008 EOS[S10] Nitrogen (solid line), ethane (dashed line); mole fraction of nitrogen $x_{\mathrm{N2}} = 0.307$ (blue), 0.945 (orange) and 0.991 mol mol^{-1} (green).

2.5.1 Simulation Results

Figure S6 shows the chemical potentials of the vapor phase along different isotherms at $p = 29\,\mathrm{bar}$. The dashed lines represent the LLE calculated from the adjusted NRTL model parameters. The VLLE is found at the intersection of the LLE and vapor phase chemical

potential for both components. An interpolation between the temperatures yields $T^{\mathrm{VLLE}} = 124.15\,\mathrm{K}$ and $y^{\mathrm{VLLE}} = 0.9986\,\mathrm{mol\,mol^{-1}}$.

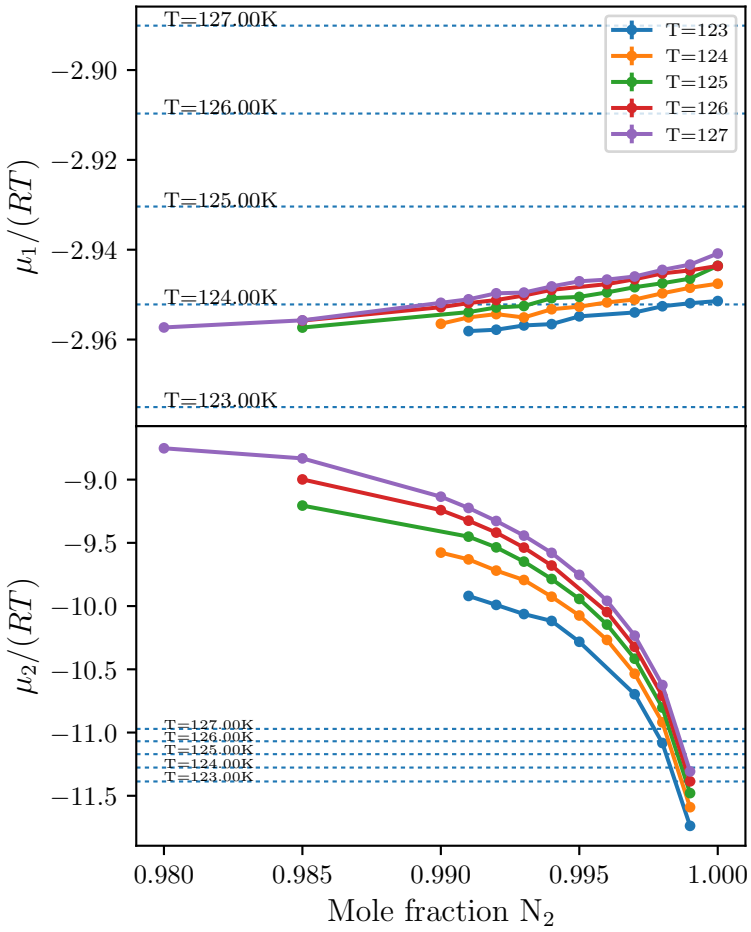

Figure S6: Chemical potentials of vapor phase as a function of nitrogen mole fraction at $p = 29\,\mathrm{bar}$ beween $T = 123$ and $T = 127\,\mathrm{K}$. The VLLE is found at the intersection between the LLE and vapor phase chemical potentials for both components; dashed lines: LLE from adjusted NRTL model at different temperatures.

3 Pressure–Mole Fraction Diagrams

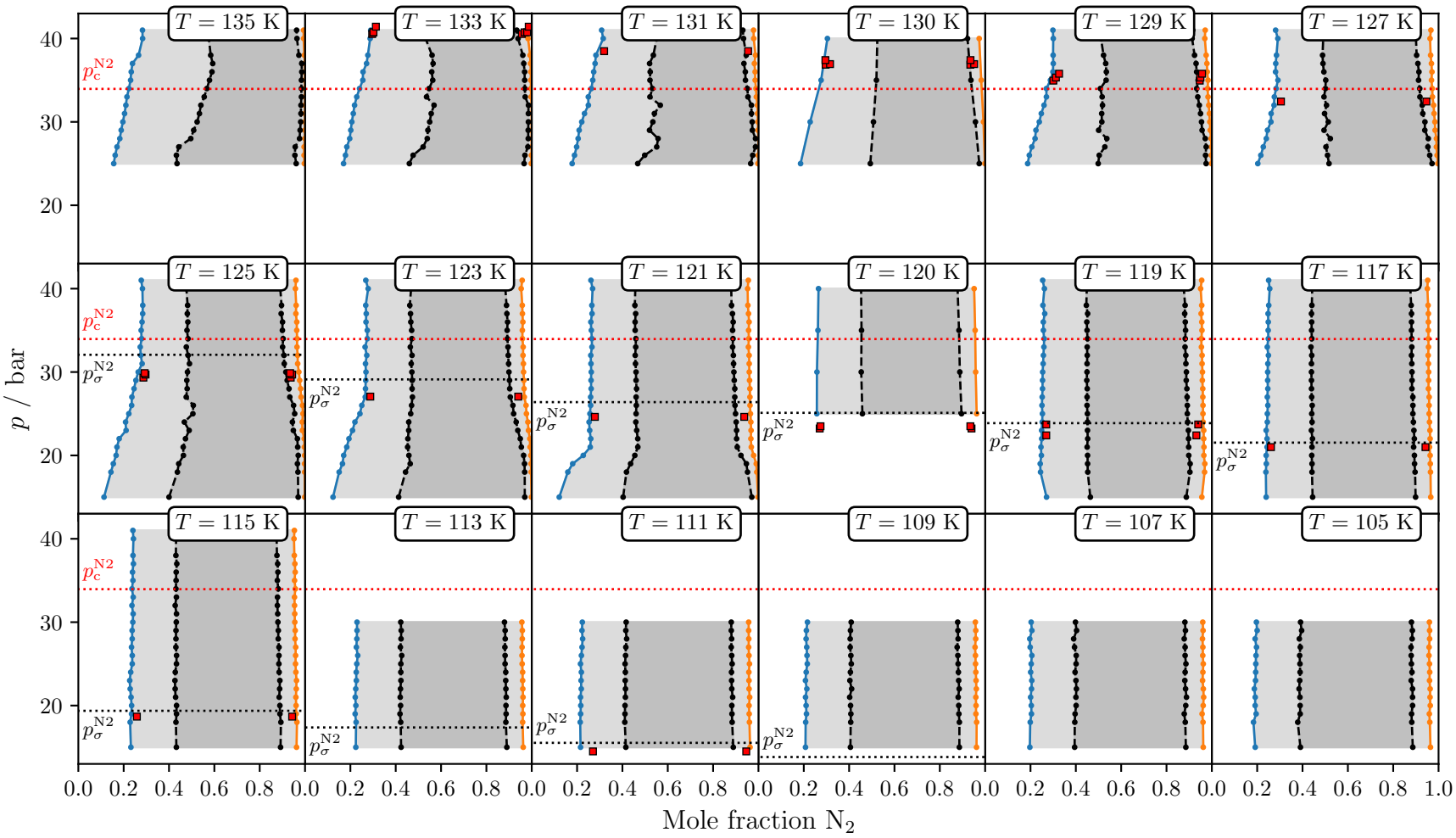

Figure S7: LLE in pressure-mole fraction phase diagrams of nitrogen + ethane at different temperatures. Critical pressure p_c and vapor pressure p_σ of nitrogen are included for orientation. Simulation results for binodal: phase I (blue) and phase II (orange); spinodals (black). Light gray: metastable region; dark gray: unstable region. Experimental data: LLE.[S15–S21]

4 Temperature–Mole Fraction Diagrams

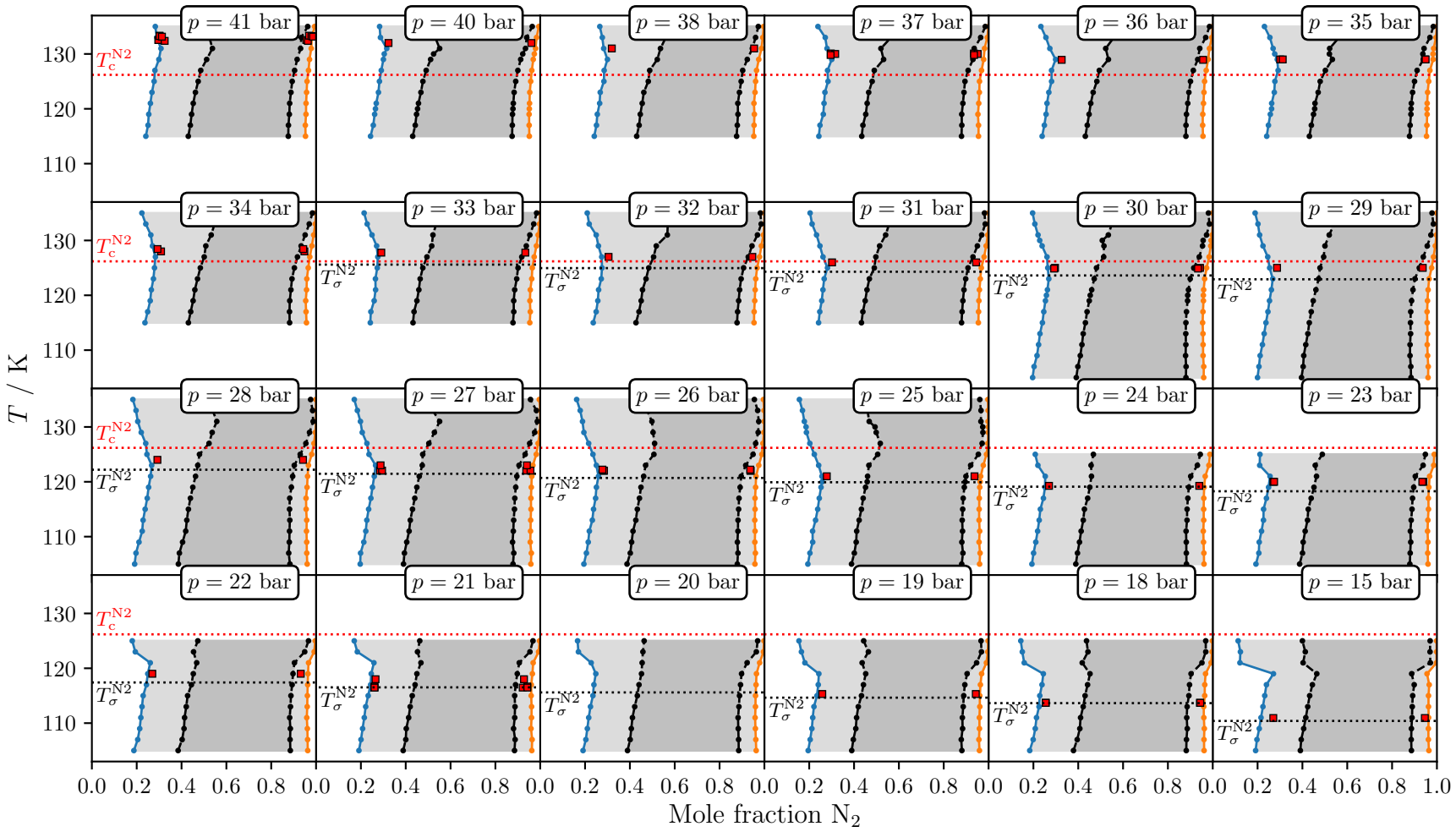

Figure S8: LLE in temperature-mole fraction phase diagrams of nitrogen + ethane at different pressures. Critical temperature T_c and boiling temperature T_σ of nitrogen are included for orientation. Simulation results for binodal: phase I (blue) and phase II (orange); spinodals (black). Light gray: metastable region; dark gray: unstable region. Experimental data: LLE.[S15–S21]

5 Tabulated LLE Results

	Mole fraction N_2 / mol mol^{-1}							
	Binodal		Spinodal		Binodal		Spinodal	
p / bar	Phase I	Phase II	Phase I	Phase II	Phase I	Phase II	Phase I	Phase II
	$T = 105$ K				$T = 107$ K			
15	0.1913	0.9643	0.3908	0.8864	0.1972	0.9621	0.3947	0.8853
18	0.1836	0.9614	0.3788	0.8819	0.1989	0.9610	0.3954	0.8828
19	0.1953	0.9594	0.3896	0.8810	0.2042	0.9569	0.3967	0.8782
20	0.1910	0.9634	0.3894	0.8854	0.2036	0.9618	0.4012	0.8849
21	0.1913	0.9624	0.3886	0.8853	0.2005	0.9638	0.4003	0.8881
22	0.1874	0.9629	0.3847	0.8853	0.2045	0.9623	0.4026	0.8841
23	0.1927	0.9602	0.3876	0.8793	0.2057	0.9590	0.4005	0.8808
24	0.1933	0.9611	0.3892	0.8829	0.2007	0.9605	0.3966	0.8822
25	0.1939	0.9600	0.3887	0.8802	0.2031	0.9621	0.4011	0.8857
26	0.1947	0.9578	0.3873	0.8793	0.2060	0.9599	0.4017	0.8821
27	0.1969	0.9583	0.3902	0.8786	0.1986	0.9604	0.3942	0.8821
28	0.1908	0.9605	0.3859	0.8835	0.1967	0.9587	0.3904	0.8781
29	0.1997	0.9605	0.3959	0.8846	0.2061	0.9613	0.4033	0.8836
30	0.1965	0.9597	0.3912	0.8805	0.2029	0.9599	0.3983	0.8811
	$T = 109$ K				$T = 111$ K			
15	0.2075	0.9619	0.4057	0.8862	0.2153	0.9629	0.4151	0.8890
18	0.2083	0.9625	0.4071	0.8864	0.2138	0.9602	0.4104	0.8840
19	0.2118	0.9593	0.4076	0.8842	0.2156	0.9592	0.4112	0.8832
20	0.2102	0.9599	0.4063	0.8834	0.2163	0.9586	0.4114	0.8826
21	0.2076	0.9590	0.4024	0.8810	0.2152	0.9613	0.4131	0.8862
22	0.2134	0.9613	0.4111	0.8854	0.2185	0.9586	0.4135	0.8823
23	0.2074	0.9600	0.4033	0.8832	0.2176	0.9583	0.4122	0.8816
24	0.2106	0.9589	0.4056	0.8820	0.2188	0.9577	0.4130	0.8811
25	0.2154	0.9577	0.4095	0.8808	0.2150	0.9603	0.4117	0.8839
26	0.2142	0.9573	0.4076	0.8796	0.2190	0.9583	0.4138	0.8821
27	0.2130	0.9555	0.4045	0.8765	0.2218	0.9568	0.4151	0.8800
28	0.2102	0.9584	0.4046	0.8807	0.2245	0.9574	0.4186	0.8816
29	0.2114	0.9586	0.4059	0.8800	0.2216	0.9568	0.4150	0.8802
30	0.2161	0.9568	0.4091	0.8788	0.2231	0.9569	0.4165	0.8801
	$T = 113$ K							
15	0.2239	0.9624	0.4237	0.8901				
18	0.2252	0.9598	0.4220	0.8858				
19	0.2210	0.9609	0.4189	0.8870				
20	0.2242	0.9602	0.4214	0.8864				
21	0.2214	0.9615	0.4198	0.8875				
22	0.2236	0.9606	0.4210	0.8860				
23	0.2263	0.9598	0.4229	0.8852				
24	0.2258	0.9598	0.4224	0.8853				
25	0.2282	0.9577	0.4226	0.8824				
26	0.2325	0.9570	0.4264	0.8824				
27	0.2264	0.9574	0.4205	0.8816				
28	0.2285	0.9584	0.4234	0.8830				
29	0.2293	0.9585	0.4242	0.8827				
30	0.2293	0.9564	0.4221	0.8798				

p / bar	Mole fraction N_2 / mol mol^{-1}							
	Binodal		Spinodal		Binodal		Spinodal	
	Phase I	Phase II	Phase I	Phase II	Phase I	Phase II	Phase I	Phase II
	$T = 115\,\mathrm{K}$				$T = 117\,\mathrm{K}$			
15	0.2319	0.9625	0.4324	0.8919	0.2395	0.9656	0.4445	0.8987
18	0.2285	0.9642	0.4305	0.8935	0.2383	0.9644	0.4416	0.8964
19	0.2347	0.9609	0.4331	0.8893	0.2403	0.9636	0.4418	0.8941
20	0.2350	0.9605	0.4332	0.8890	0.2395	0.9628	0.4406	0.8936
21	0.2325	0.9596	0.4290	0.8860	0.2435	0.9601	0.4417	0.8901
22	0.2287	0.9614	0.4270	0.8880	0.2434	0.9627	0.4439	0.8932
23	0.2267	0.9624	0.4261	0.8890	0.2395	0.9620	0.4391	0.8913
24	0.2310	0.9596	0.4275	0.8857	0.2446	0.9601	0.4421	0.8891
25	0.2378	0.9580	0.4328	0.8847	0.2448	0.9585	0.4406	0.8868
26	0.2378	0.9584	0.4332	0.8850	0.2470	0.9583	0.4426	0.8868
27	0.2345	0.9588	0.4303	0.8851	0.2446	0.9586	0.4404	0.8866
28	0.2376	0.9559	0.4306	0.8818	0.2469	0.9554	0.4395	0.8826
29	0.2373	0.9566	0.4308	0.8821	0.2462	0.9562	0.4394	0.8832
30	0.2402	0.9548	0.4320	0.8803	0.2463	0.9563	0.4393	0.8829
31	0.2417	0.9545	0.4330	0.8795	0.2470	0.9554	0.4393	0.8820
32	0.2364	0.9537	0.4271	0.8781	0.2495	0.9543	0.4406	0.8805
33	0.2420	0.9535	0.4325	0.8785	0.2445	0.9558	0.4371	0.8820
34	0.2367	0.9573	0.4305	0.8821	0.2489	0.9554	0.4408	0.8816
35	0.2408	0.9537	0.4312	0.8779	0.2485	0.9552	0.4399	0.8805
36	0.2389	0.9566	0.4316	0.8803	0.2489	0.9551	0.4403	0.8807
37	0.2430	0.9551	0.4343	0.8792	0.2479	0.9551	0.4395	0.8807
38	0.2410	0.9527	0.4303	0.8761	0.2510	0.9539	0.4412	0.8792
40	0.2430	0.9513	0.4311	0.8746	0.2553	0.9506	0.4425	0.8755
41	0.2407	0.9530	0.4301	0.8761	0.2505	0.9522	0.4392	0.8768
	$T = 119\,\mathrm{K}$				$T = 121\,\mathrm{K}$			
15	0.2708	0.9559	0.4641	0.8874	0.1213	0.9980	0.4030	0.9707
18	0.2443	0.9679	0.4525	0.9033	0.1591	0.9926	0.4178	0.9518
19	0.2429	0.9689	0.4519	0.9042	0.1806	0.9904	0.4360	0.9468
20	0.2480	0.9646	0.4518	0.8981	0.2272	0.9788	0.4547	0.9228
21	0.2462	0.9651	0.4498	0.8977	0.2844	0.9567	0.4779	0.8904
22	0.2494	0.9640	0.4524	0.8973	0.2604	0.9665	0.4676	0.9037
23	0.2490	0.9641	0.4515	0.8965	0.2556	0.9674	0.4629	0.9036
24	0.2518	0.9615	0.4515	0.8933	0.2529	0.9664	0.4590	0.9018
25	0.2526	0.9607	0.4512	0.8918	0.2567	0.9647	0.4603	0.8991
26	0.2506	0.9609	0.4494	0.8918	0.2599	0.9627	0.4613	0.8967
27	0.2517	0.9602	0.4496	0.8908	0.2598	0.9624	0.4603	0.8956
28	0.2531	0.9599	0.4502	0.8899	0.2621	0.9622	0.4624	0.8956
29	0.2532	0.9580	0.4483	0.8870	0.2616	0.9608	0.4602	0.8932
30	0.2537	0.9585	0.4492	0.8878	0.2626	0.9595	0.4600	0.8917
31	0.2558	0.9569	0.4495	0.8855	0.2612	0.9592	0.4576	0.8903
32	0.2569	0.9569	0.4503	0.8852	0.2604	0.9589	0.4563	0.8895
33	0.2592	0.9540	0.4499	0.8817	0.2656	0.9557	0.4586	0.8861
34	0.2602	0.9539	0.4515	0.8827	0.2652	0.9577	0.4593	0.8879
35	0.2569	0.9564	0.4495	0.8841	0.2629	0.9565	0.4561	0.8860
36	0.2565	0.9556	0.4484	0.8828	0.2607	0.9587	0.4559	0.8886
37	0.2628	0.9526	0.4521	0.8802	0.2660	0.9562	0.4584	0.8855
38	0.2547	0.9553	0.4463	0.8821	0.2651	0.9534	0.4549	0.8814
40	0.2613	0.9504	0.4483	0.8763	0.2685	0.9523	0.4568	0.8800
41	0.2538	0.9552	0.4448	0.8808	0.2611	0.9554	0.4521	0.8823

	Mole fraction N_2 / mol mol^{-1}							
	Binodal		Spinodal		Binodal		Spinodal	
p / bar	Phase I	Phase II	Phase I	Phase II	Phase I	Phase II	Phase I	Phase II
	$T = 123$ K				$T = 125$ K			
15	0.1011	1.0000	0.4898	0.9938	0.0991	1.0000	0.4496	0.9899
18	0.1432	1.0000	0.5700	0.9946	0.1264	1.0000	0.5288	0.9934
19	0.1874	0.9769	0.1874	0.9998	0.1474	1.0000	0.5690	0.9943
20	0.1615	0.9816	0.1615	0.9998	0.1700	1.0000	0.5829	0.9937
21	0.1841	0.9927	0.4525	0.9541	0.1777	1.0000	0.6200	0.9944
22	0.1936	0.9916	0.4535	0.9494	0.1847	1.0000	0.6167	0.9946
23	0.2095	0.9856	0.4572	0.9384	0.3377	1.0000	0.3028	0.9958
24	0.2200	0.9829	0.4573	0.9315	0.4183	0.9962	0.7230	0.9774
25	0.2421	0.9766	0.4661	0.9201	0.3876	0.9949	0.7021	0.9735
26	0.2504	0.9748	0.4700	0.9168	0.2351	0.9887	0.5071	0.9495
27	0.2656	0.9672	0.4737	0.9054	0.2362	0.9824	0.4759	0.9328
28	0.2666	0.9660	0.4722	0.9029	0.2456	0.9806	0.4799	0.9293
29	0.2677	0.9653	0.4725	0.9020	0.2539	0.9764	0.4784	0.9213
30	0.2687	0.9639	0.4712	0.8995	0.2641	0.9727	0.4814	0.9153
31	0.2667	0.9632	0.4682	0.8980	0.2913	0.9646	0.4955	0.9045
32	0.2723	0.9615	0.4719	0.8963	0.2756	0.9675	0.4841	0.9072
33	0.2649	0.9622	0.4644	0.8952	0.2730	0.9646	0.4762	0.9011
34	0.2746	0.9589	0.4713	0.8927	0.2792	0.9651	0.4837	0.9034
35	0.2746	0.9585	0.4702	0.8915	0.2771	0.9635	0.4792	0.9002
36	0.2688	0.9609	0.4665	0.8935	0.2811	0.9636	0.4830	0.9007
37	0.2700	0.9589	0.4652	0.8904	0.2838	0.9596	0.4807	0.8947
38	0.2677	0.9582	0.4621	0.8887	0.2841	0.9608	0.4820	0.8964
40	0.2784	0.9534	0.4678	0.8836	0.2828	0.9575	0.4766	0.8908
41	0.2680	0.9579	0.4619	0.8881	0.2776	0.9600	0.4742	0.8936
	$T = 120$ K				$T = 130$ K			
25	0.2576	0.9626	0.4585	0.8957	0.1850	0.9999	0.5451	0.9879
30	0.2580	0.9582	0.4535	0.8883	0.2396	0.9998	0.6673	0.9909
35	0.2624	0.9558	0.4547	0.8846	0.2764	0.9827	0.5204	0.9374
40	0.2650	0.9514	0.4528	0.8784	0.3042	0.9737	0.5244	0.9221

	Mole fraction N_2 / mol mol^{-1}							
	Binodal		Spinodal		Binodal		Spinodal	
p / bar	Phase I	Phase II	Phase I	Phase II	Phase I	Phase II	Phase I	Phase II
	$T = 127$ K				$T = 129$ K			
25	0.2324	0.9997	0.7038	0.9909	0.1940	1.0000	0.5691	0.9904
26	0.5015	0.9987	0.2582	0.9871	0.2008	1.0000	0.5843	0.9912
27	0.6326	0.9998	0.2255	0.9942	0.2083	0.9999	0.5955	0.9910
28	0.2402	0.9907	0.5226	0.9547	0.2368	0.9999	0.7028	0.9927
29	0.2590	0.9869	0.5263	0.9469	0.2830	0.9996	0.7176	0.9899
30	0.3180	0.9892	0.6155	0.9573	0.3732	0.9969	0.7066	0.9787
31	0.3174	0.9873	0.5988	0.9527	0.2839	0.9931	0.5990	0.9645
32	0.2743	0.9783	0.5057	0.9280	0.2597	0.9864	0.5177	0.9447
33	0.2757	0.9731	0.4946	0.9177	0.2702	0.9831	0.5160	0.9379
34	0.2834	0.9721	0.5010	0.9170	0.3244	0.9885	0.6059	0.9552
35	0.2916	0.9688	0.5023	0.9117	0.3085	0.9822	0.5587	0.9404
36	0.2810	0.9709	0.4941	0.9134	0.2990	0.9795	0.5346	0.9330
37	0.2818	0.9686	0.4902	0.9088	0.3005	0.9782	0.5317	0.9304
38	0.2851	0.9650	0.4883	0.9033	0.2998	0.9749	0.5222	0.9237
40	0.2910	0.9625	0.4912	0.9003	0.3004	0.9689	0.5111	0.9129
41	0.2812	0.9663	0.4856	0.9044	0.2989	0.9707	0.5120	0.9156
	$T = 131$ K				$T = 133$ K			
25	0.1794	0.9998	0.5278	0.9856	0.1709	0.9997	0.5076	0.9829
26	0.1878	0.9999	0.5416	0.9868	0.1788	0.9997	0.5140	0.9825
27	0.1980	0.9999	0.5512	0.9870	0.1843	0.9997	0.5208	0.9829
28	0.2047	0.9999	0.5572	0.9871	0.1969	0.9998	0.5391	0.9846
29	0.2106	0.9999	0.5806	0.9888	0.2017	0.9997	0.5419	0.9843
30	0.2210	0.9998	0.6063	0.9892	0.2064	0.9998	0.5498	0.9853
31	0.2436	0.9996	0.6511	0.9884	0.2127	0.9997	0.5565	0.9852
32	0.2893	0.9997	0.7198	0.9907	0.2184	0.9997	0.5690	0.9856
33	0.5690	0.9984	0.7989	0.9870	0.2314	0.9997	0.6181	0.9881
34	0.5178	0.9974	0.7687	0.9826	0.2496	0.9995	0.6406	0.9873
35	0.3064	0.9895	0.5926	0.9564	0.2822	0.9994	0.6861	0.9881
36	0.3260	0.9909	0.6141	0.9604	0.2809	0.9994	0.6714	0.9874
37	0.4269	0.9917	0.6928	0.9664	0.4335	0.9988	0.7509	0.9864
38	0.3703	0.9893	0.6433	0.9588	0.4483	0.9977	0.7421	0.9826
40	0.3153	0.9792	0.5513	0.9342	0.4086	0.9927	0.6876	0.9681
41	0.3082	0.9785	0.5377	0.9310	0.4360	0.9912	0.6934	0.9654
	$T = 135$ K							
25	0.1561	0.9970	0.4353	0.9610				
26	0.1625	0.9957	0.4325	0.9553				
27	0.1706	0.9959	0.4432	0.9566				
28	0.1829	0.9991	0.4959	0.9758				
29	0.1890	0.9993	0.5088	0.9783				
30	0.1964	0.9995	0.5239	0.9808				
31	0.2038	0.9996	0.5341	0.9819				
32	0.2097	0.9995	0.5405	0.9821				
33	0.2144	0.9996	0.5552	0.9840				
34	0.2230	0.9995	0.5669	0.9838				
35	0.2305	0.9994	0.5785	0.9840				
36	0.2334	0.9995	0.5895	0.9857				
37	0.2389	0.9995	0.5928	0.9853				
38	0.2776	0.9993	0.6568	0.9861				
40	0.3561	0.9981	0.7000	0.9824				
41	0.3908	0.9973	0.7080	0.9800				

References

(S1) Vrabec, J.; Hasse, H. Grand Equilibrium: vapour-liquid equilibria by a new molecular simulation method. *Mol. Phys.* **2002**, *100*, 3375–3383.

(S2) Kirkwood, J. G.; Buff, F. P. The Statistical Mechanical Theory of Solutions. I. *J. Chem. Phys.* **1951**, *19*, 774–777.

(S3) Deublein, S.; Eckl, B.; Stoll, J.; Lishchuk, S. V.; Guevara-Carrion, G.; Glass, C. W.; Merker, T.; Bernreuther, M.; Hasse, H.; Vrabec, J. ms2: A molecular simulation tool for thermodynamic properties. *Comput. Phys. Commun.* **2011**, *182*, 2350–2367.

(S4) Glass, C. W.; Reiser, S.; Rutkai, G.; Deublein, S.; Köster, A.; Guevara-Carrion, G.; Wafai, A.; Horsch, M.; Bernreuther, M.; Windmann, T.; Hasse, H.; Vrabec, J. ms2: A molecular simulation tool for thermodynamic properties, new version release. *Comput. Phys. Commun.* **2014**, *185*, 3302–3306.

(S5) Rutkai, G.; Köster, A.; Guevara-Carrion, G.; Janzen, T.; Schappals, M.; Glass, C. W.; Bernreuther, M.; Wafai, A.; Stephan, S.; Kohns, M.; Reiser, S.; Deublein, S.; Horsch, M.; Hasse, H.; Vrabec, J. ms2: A molecular simulation tool for thermodynamic properties, release 3.0. *Comput. Phys. Commun.* **2017**, *221*, 343–351.

(S6) Fingerhut, R.; Guevara-Carrion, G.; Nitzke, I.; Saric, D.; Marx, J.; Langenbach, K.; Prokopev, S.; Celný, D.; Bernreuther, M.; Stephan, S.; Kohns, M.; Hasse, H.; Vrabec, J. ms2: A molecular simulation tool for thermodynamic properties, release 4.0. *Comput. Phys. Commun.* **2021**, *262*, 107860.

(S7) Fingerhut, R.; Vrabec, J. Kirkwood-Buff integration: A promising route to entropic properties? *Fluid Phase Equilib.* **2019**, *485*, 270–281.

(S8) Widom, B. Some Topics in the Theory of Fluids. *J. Chem. Phys.* **1963**, *39*, 2808–2812.

(S9) Lemmon, E. W.; Bell, I.; Huber, M. L.; McLinden, M. O. NIST Standard Reference Database 23: Reference Fluid Thermodynamic and Transport Properties-REFPROP, Version 10.0, National Institute of Standards and Technology. 2018.

(S10) Kunz, O.; Wagner, W. The GERG-2008 Wide-Range Equation of State for Natural Gases and Other Mixtures: An Expansion of GERG-2004. *J. Chem. Eng. Data* **2012**, *57*, 3032–3091.

(S11) Guevara-Carrion, G.; Janzen, T.; Muñoz-Muñoz, Y. M.; Vrabec, J. Mutual diffusion of binary liquid mixtures containing methanol, ethanol, acetone, benzene, cyclohexane, toluene, and carbon tetrachloride. *J. Chem. Phys.* **2016**, *144*, 124501.

(S12) Tsuboka, T.; Katayama, T. Modified Wilson equation for vapor-liquid and liquid-liquid equilibria. *J. Chem. Eng. Jpn.* **1975**, *8*, 181–187.

(S13) Nagata, I.; Tamura, K.; Yamada, T. Correlation of liquid-liquid equilibria in aqueous and organic systems using a modified Wilson model. *J. Solution Chem.* **1996**, *25*, 567–587.

(S14) Maurer, G.; Prausnitz, J. On the derivation and extension of the UNIQUAC equation. *Fluid Phase Equilib.* **1978**, *2*, 91–99.

(S15) Chang, S.-D.; Lu, B. C. Vapor-liquid equilibriums in the nitrogen-methane-ethane system. *Chemical Engineering Progress Symposium Series* **1967**, *63*, 18–27.

(S16) Lu, B.; Chang, S.; Elshayal, I.; Yu, P.; Gravelle, D.; Poon, D. Low temperature phase equilibria of natural gas components. Proc. 1st Int. Conf. Calorimetry and Thermodynamics, Warsaw. 1969; p 775.

(S17) Yu, P.; Elshayal, I. M.; Lu, B. C.-Y. Liquid-liquid-vapor equilibria in the nitrogen-methane-ethane system. *Can. J. Chem. Eng.* **1969**, *47*, 495–498.

(S18) Gasem, K.; Hiza, M.; Kidnay, A. Phase behavior in the nitrogen + ethylene system from 120 to 200 K. *Fluid Phase Equilib.* **1981**, *6*, 181–189.

(S19) Kremer, H.; Knapp, H. Three-phase conditions are predictable. *Hydrocarbon Process.* **1983**, *62*, 79–83.

(S20) Kohn, J. P.; Llave, F.; Luks, K. D. *Liquid-liquid-vapor Equilibria in Cryogenic LNG Mixtures, Phase IV: Nitrogen Rich Systems*; Gas Processors Association, 1984.

(S21) Guedes, H. J.; Zollweg, J. A.; Filipe, E. J.; Martins, L. F.; Calado, J. C. Thermodynamics of liquid (nitrogen + ethane). *J. Chem. Thermodyn.* **2002**, *34*, 669–678.